Roles of Cellular NSF Protein in Entry and Nuclear Egress of Budded Virions of Autographa californica Multiple Nucleopolyhedrovirus

Ya Guo,[a] Qi Yue,[a] Jinli Gao,[a] Zhe Wang,[a] Yun-Ru Chen,[b*] Gary W. Blissard,[b] Tong-Xian Liu,[a] Zhaofei Li[a]

State Key Laboratory of Crop Stress Biology for Arid Areas, Key Laboratory of Northwest Loess Plateau Crop Pest Management of Ministry of Agriculture, College of Plant Protection, Northwest A&F University, Yangling, Shaanxi, China[a]; Boyce Thompson Institute, Cornell University, Ithaca, New York, USA[b]

ABSTRACT In eukaryotic cells, the soluble N-ethylmaleimide-sensitive factor (NSF) attachment protein receptor (SNARE) proteins comprise the minimal machinery that triggers fusion of transport vesicles with their target membranes. Comparative studies revealed that genes encoding the components of the SNARE system are highly conserved in yeast, insect, and human genomes. Upon infection of insect cells by the virus Autographa californica multiple nucleopolyhedrovirus (AcMNPV), the transcript levels of most SNARE genes initially were upregulated. We found that overexpression of dominant-negative (DN) forms of NSF or knockdown of the expression of NSF, the key regulator of the SNARE system, significantly affected infectious AcMNPV production. In cells expressing DN NSF, entering virions were trapped in the cytoplasm or transported to the nucleus with low efficiency. The presence of DN NSF also moderately reduced trafficking of the viral envelope glycoprotein GP64 to the plasma membrane but dramatically inhibited production of infectious budded virions (BV). Transmission electron microscopy analysis of infections in cells expressing DN NSF revealed that progeny nucleocapsids were retained in a perinuclear space surrounded by inner and outer nuclear membranes. Several baculovirus conserved (core) proteins (Ac76, Ac78, GP41, Ac93, and Ac103) that are important for infectious budded virion production were found to associate with NSF, and NSF was detected within the assembled BV. Together, these data indicate that the cellular SNARE system is involved in AcMNPV infection and that NSF is required for efficient entry and nuclear egress of budded virions of AcMNPV.

IMPORTANCE Little is known regarding the complex interplay between cellular factors and baculoviruses during viral entry and egress. Here, we examined the cellular SNARE system, which mediates the fusion of vesicles in healthy cells, and its relation to baculovirus infection. Using a DN approach and RNA interference knockdown, we demonstrated that a general disruption of the SNARE machinery significantly inhibited the production of infectious BV of AcMNPV. The presence of a DN NSF protein resulted in low-efficiency entry of BV and the retention of progeny nucleocapsids in the perinuclear space during egress. Combined with these effects, we also found that several conserved (core) baculovirus proteins closely associate with NSF, and these results suggest their involvement in the egress of BV. Our findings are the first to demonstrate that the SNARE system is required for efficient entry of BV and nuclear egress of progeny nucleocapsids of baculoviruses.

KEYWORDS SNARE, NSF, baculovirus, AcMNPV, virus entry and egress

In eukaryotic cells, soluble N-ethylmaleimide-sensitive factor (NSF) attachment protein receptor (SNARE) proteins constitute the minimal machinery that mediates the fusion of transport vesicles with target membranes (1, 2). These evolutionarily conserved SNARE proteins constitute a large family of approximately 50 or more proteins in mammals and are classified as either v-SNAREs (found on vesicle membranes) or t-SNAREs (found on target membranes) (1). During the membrane fusion process, a highly stable four-helix bundle is formed from an interaction of the v-SNARE and t-SNARE proteins that are anchored in opposing membranes. Most v-SNARE and t-SNARE protein encodes a 50- to 60-amino-acid SNARE motif, a motif that contains a heptad repeat that forms a coiled-coil structure. Four SNARE proteins, called SNAP-23 (synaptosome-associated protein of 23 kDa), SNAP-25, SNAP-29, and SNAP-47, each contain two tandem SNARE motifs separated by a linker region. The coiled-coil structures from each of four v-SNAREs and four t-SNAREs interact to form the four-helix bundle during fusion. The center of the four-helix bundle contains 16 stacked layers of interacting side chains, which are largely hydrophobic, except for a central "0" layer that contains three highly conserved glutamine (Q) residues and one highly conserved arginine (R) residue, each contributed by one of the subunit proteins (see Fig. 2 in reference 1). Based on these conserved residues and the similarity of SNARE motifs, SNARE proteins are classified into four main types: Qa-SNAREs (SNAREs containing a SNARE motif that is close to that of syntaxin 1, 2, 3, 4, 5, 7, 11, 13, 16, 17, or 18), Qb-SNAREs (SNAREs containing a SNARE motif that is similar to the N-terminal SNARE motif of SNAP-25), Qc-SNAREs (SNAREs containing a SNARE motif that is similar to the C-terminal SNARE motif of SNAP-25), and R-SNAREs (SNAREs containing a SNARE motif that is close to that of vesicle-associated membrane proteins [VAMP]). Functional SNARE complexes that drive membrane fusion need one of each of the above-described four SNARE types (1, 3). These four main types of SNARE proteins can be further classified into 20 different conserved groups which participate in diverse intracellular trafficking processes (4). At a late step of membrane fusion, SNARE complexes are disassembled into individual SNARE proteins for recycling (1). This disassembly process is catalyzed by a protein called N-ethylmaleimide-sensitive factor and its adaptor protein, α-soluble NSF attachment protein (α-SNAP) (5–7). NSF is an ATPase that belongs to the AAA+ ATPase family, a family of proteins that are involved in a variety of cellular activities (8). NSF functions as a homohexamer, and each subunit consists of the N-terminal domain (NSF-N) and two AAA+ domains (NSF-D1 and NSF-D2). The N domain is required for interaction with the α-SNAP–SNARE complex. The D1 domain provides ATPase activity associated with SNARE disassembly, and the D2 domain is involved in nucleotide-dependent hexamerization (9–11). Two well-characterized mutations of NSF (NSF^{E329Q} and NSF^{R385A}) result in failure of NSF to bind or hydrolyze ATP. Inactivation of NSF function by overexpressing these dominant-negative (DN) forms of NSF leads to failure in disassembly of SNARE complexes and consequent disruption of SNARE function (10, 12, 13).

A number of studies have demonstrated an important role of the cellular SNARE machinery in the replication of certain mammalian viruses. In human cytomegalovirus (HCMV)-infected cells, SNARE protein SNAP-23 is found in the region of viral assembly in the cytoplasm, and depletion of SNAP-23 by RNA interference (RNAi) significantly reduced infectious HCMV production and disrupted virion assembly or maturation (14). For another herpesvirus, human herpesvirus 6 (HHV-6), viral glycoproteins M and N (gM/gN) interact with VAMP3, a SNARE involved in vesicular transport. During the late phase of virus infection, the expression level of VAMP3 was significantly upregulated and VAMP3 became incorporated into mature HHV-6 virions (15). The interaction of a viral protein with host SNARE system components was also reported in cells infected with human parainfluenza virus type 3 (HPIV3). The HPIV3 phosphoprotein (P) interacts with SNAP-29, and through this interaction, HPIV3 induces incomplete autophagy by inhibiting the interaction of SNAP-29 with syntaxin 17 (Syx17), a SNARE associated with autophagosome-lysosome fusion (16). Additionally, downregulation of Syx17 and impairment of autophagosome-lysosome fusion by hepatitis C virus (HCV) are critical for

HCV release (17). In another example of the requirement for SNARE protein functions in viral infections, it was found that overexpression of DN NSF (NSF^{E329Q}) substantially reduced production of infectious human immunodeficiency virus type 1 (HIV-1), and this results from reduced levels of Gag at the plasma membrane (18, 19). In addition to the role of SNARE proteins in efficient assembly or egress of viruses, SNARE proteins are also involved in viral entry in many cases. Inhibition of VAMP8 (a SNARE protein that participates in endosomal fusion) significantly decreases influenza A virus and vesicular stomatitis virus (VSV) entry into host cells (20). Inactivation of VAMP3 also results in defects in bunyavirus (Uukuniemi virus) entry (21).

Baculoviruses represent a family of large double-stranded DNA viruses with circular genomes that range from 80 to 180 kb. Many baculoviruses are highly pathogenic to their insect hosts (22). These viruses are widely used as biological insecticides, protein expression vectors, and mammalian cell transduction vectors (23–25). During the infection cycle, baculoviruses produce two types of virions: occlusion-derived virions (ODV) and budded virions (BV). ODV and BV are identical in genomic DNA content and nucleocapsid structure. However, they differ in the source and composition of their envelopes and in their functional roles in the infection cycle in the animal. ODV are acquired orally and initiate the primary infection in the midgut epithelium. Within midgut epithelial cells, BV are produced by budding from the cell surface. BV spread the viral infection from cell to cell within the infected insect. BV obtain the virion envelope from the plasma membrane, whereas ODV assemble in the nucleus and acquire their envelopes from virus-induced intranuclear microvesicles, which are derived from the inner nuclear membrane (INM) (22). *Autographa californica multiple nucleopolyhedrovirus* (AcMNPV) is the best-studied baculovirus and is the type species of the *Baculoviridae*. BV of AcMNPV enter host cells via clathrin-mediated endocytosis (26). The major viral envelope glycoprotein, GP64, is essential for receptor binding and low-pH-triggered membrane fusion (27). During entry, the acidification of endosomes triggers a conformational change in GP64, which then mediates fusion of the viral envelope and endosomal membranes, releasing the nucleocapsid into the cytosol (28). Nucleocapsids are then transported to the nuclear periphery via actin-based motility (29) and enter the nucleus through the nuclear pore complex (22, 30). After the viral genome is released within the nucleus, viral transcription and DNA replication occur and are subsequently followed by progeny nucleocapsid assembly in a dense region referred to as the virogenic stroma (VS) (22). Some progeny nucleocapsids exit the nucleus. During this egress from the nucleus, nucleocapsids appear to acquire an envelope by blebbing of the nuclear membranes (31). This double envelope (derived presumably from inner and outer nuclear membranes) appears to be lost in the cytosol, as naked nucleocapsids are frequently observed in the cytosol and in the process of budding at the plasma membrane (22, 31). Because enveloped virions found within the cytosol represent a virus-induced vesicle, the loss of the double envelope within the cytosol may involve a fusion process that could be mediated by the cellular SNARE system. Intriguingly, several host proteins involved in vesicular transport have been identified in purified budded virions of AcMNPV by mass spectrometry (32).

To investigate whether the host cellular SNARE machinery is required for AcMNPV infection, we first analyzed the transcript levels of the SNARE genes in AcMNPV-infected insect cells (33) and found that most of the SNARE transcripts were upregulated upon AcMNPV infection. We cloned the NSF gene from Sf9 cells, generated dominant-negative forms of Sf9 NSF, and analyzed the effects of DN NSF proteins on AcMNPV BV entry, viral replication, and BV egress. Our results demonstrated that NSF is required for efficient entry of AcMNPV BV into Sf9 cells and for egress of BV. In addition, we found that NSF associates with several conserved (core) viral proteins, suggesting that NSF associations with viral proteins are involved in egress or assembly of AcMNPV BV.

RESULTS

Expression profiles of SNARE genes upon AcMNPV infection. As a first step, we performed a comprehensive comparison of SNARE protein components in yeast,

humans, and insects. We found that most of the components of the cellular SNARE machinery are evolutionarily conserved across these eukaryotic species (Table 1). Insect genes encoding SNARE components appear to more closely mirror the yeast genome in terms of SNARE gene numbers. In contrast to the rather large expansion of SNARE genes observed in the human genome, we identified only one SNARE gene (the ortholog of yeast Sec17) that was expanded in the six insect orders (Table 1). In addition, several yeast SNARE genes were not identified in insect genomes, and these include Sft1, Vam3, Vam7, and Snc1/Snc2. In a recent transcriptome analysis of AcMNPV-infected *Trichoplusia ni* cells (Tnms42), expression profiles were generated for host genes throughout the AcMNPV infection cycle (33). We therefore analyzed the expression profiles of host SNARE gene orthologs (Fig. 1; see also Table S1 in the supplemental material) in uninfected and AcMNPV-infected cells. Upon AcMNPV infection, more than 70% of the SNARE genes (17/23) were upregulated (>1-fold change in transcript abundance upon AcMNPV infection). Of these genes, the expression levels of Bet1, Sec20, Sec22, SNAP-29, Syb, and Use1 were increased >2-fold in AcMNPV-infected cells. Overall, we found that in the early stages of AcMNPV infection, most of the SNARE genes were either upregulated or maintained their expression levels (Fig. 1; Table S1).

In eukaryotic cells, NSF forms a regulatory complex with α-SNAP to unfold and recycle SNARE proteins (9). Although the α-SNAP transcript is upregulated in the very early stage of AcMNPV infection (1 to 6 h postinfection [p.i.]) in *T. ni* cells, the transcript level of NSF remained stable and slightly decreased by 6 h p.i. (Fig. 1E; Table S1). To determine the transcript levels of NSF in AcMNPV-infected Sf9 cells, we first identified the Sf9 NSF mRNA (from SPODOBASE) and used quantitative real-time PCR (qRT-PCR) to measure NSF transcript levels from uninfected and infected Sf9 at various times postinfection. As shown in Fig. 2, AcMNPV infection significantly upregulated the transcript levels of NSF at 1 and 3 h p.i. Similar to observations in AcMNPV-infected Tnms42 cells, the transcript levels of NSF were substantially decreased at 6 h p.i. Combined, these transcript data suggest that the cellular SNARE system is important in AcMNPV infection or that specific SNARE components play important roles.

Analysis of NSF from Sf9 cells. Because the SNARE system may be important for successful AcMNPV infection, we asked whether NSF, a key regulator of SNARE activity, is required for AcMNPV replication. To isolate the NSF gene from Sf9 cells, we designed gene-specific primers targeting the 5' and 3' ends of the NSF open reading frame (ORF) based on partial expressed sequence tag (EST) sequences of *Spodoptera frugiperda* NSF obtained from BLAST searches. We then amplified and cloned the NSF ORF from Sf9 cells. The Sf9 NSF gene contains a 2,241-bp ORF encoding a 746-amino-acid protein with a predicted molecular mass of 82.6 kDa. Sf9 NSF had highest amino acid sequence identity to NSF of *Bombyx mori* (92.25%) and is highly conserved with orthologs from other insect species (71.64% to 78.51%) and other eukaryotes (44.77% similar to yeast NSF and 63.19% similar to human NSF). Mammalian NSF proteins contain several functional domains: an amino-terminal domain (NSF-N) followed by two homologous domains, termed D1 and D2. These functional domains were predicted to be present in NSF of *Spodoptera frugiperda* (Sf9 cells) and other insects (Fig. S1).

Transient expression of WT and DN NSF in Sf9 cells. To generate dominant-negative (DN) forms of Sf9 NSF proteins, two previously characterized point mutations (E329Q and R385A) that each abolish ATP hydrolysis activity in human NSF (10, 12) were introduced into Sf9 NSF (Fig. 3A; Fig. S1, NSF^{E329Q} and NSF^{R385A}). To confirm the expression and subcellular localization of NSF constructs, wild-type (WT) and DN NSFs were fused with green fluorescent protein (GFP) at the C terminus and inserted into a plasmid under the control of an AcMNPV *ie1* promoter. These constructs were transiently expressed in Sf9 cells (Fig. 3B and C). A plasmid expressing GFP under the same promoter (gfppBlue) was used as a control. Transient expression of each construct was confirmed by Western blotting with an anti-GFP antibody (Fig. 3B) and by epifluorescence and confocal microscopies (Fig. 3C). GFP-tagged WT NSF was distributed diffusely throughout the cytoplasm. In contrast, NSF^{E329Q}-GFP and NSF^{R385A}-GFP showed a

TABLE 1 SNARE proteins in yeast, human, and insects

Function site and classification	SNARE protein by species[i]		
	Yeast	Human	Insect[a]
Endosome/lysosome			
Qa	Pep12	Syx7	+
	Vam3	−	−
	−	Syx13	−
	−	Syx17	+[c]
	−	Syx20	+[d]
Qb	Vti1	Vti1a	Vti1[e]
		Vti1b	
Qc	Syx8	Syx8	+[f]
	Tlg1	Syx6	+
	−	Syx10	−
	Vam7	−	−
R	Nyv1	VAMP7	+
	−	Endob/VAMP8	−
	−	VAMP4	+[g]
Endoplasmic reticulum			
Qa	Ufe1	Syx18	+
Qb	Sec20	Sec20	+
Qc	Slt1/Use1	Use1	+
R	Sec22	Sec22a	Sec22
	−	Sec22b	
	−	Sec22c	
Golgi apparatus			
Qa	Sed5	Syx5	+
	Tlg2	Syx16	+
Qb	Bos1	Memb	+
	Gos1	Gos28	+
Qc	Bet1	Bet1	+
	Sft1	Gos15	−
R	Ykt6	Ykt6	+
Polarization			
R	−	Amisyn	−
		Tom1	Tom
	−	Tom2	
	Sro7/Sro77	Lgl1	Lgl
		Lgl2	
Regulatory complex	Sec17	α − SNAP	+
		β − SNAP	−
		γ − SNAP	+
	Sec18	NSF	+
Secretion pathway			
Qa	Sso1/Sso2	Syx1a	Syx1
		Syx1b	
	−	Syx2	−
	−	Syx3	−
	−	Syx4	+[h]
	−	Syx11	−
	−	Syx19	−
Qbc[b]	Sec9	SNAP-25a	SNAP-25
	SPO20	SNAP-25b	
	−	SNAP-23	−
	−	SNAP-29	+
	−	SNAP-47	−
R	Snc1/Snc2−	Syb1	Syb
		Syb2	
		Syb3	
		Myob	−

[a]Insects represent sequenced insect genomes, which include those of *Acyrthosiphon pisum, Aedes aegypti, Anopheles gambiae, Apis mellifera, Bombyx mori, Culex quinquefasciatus, Danaus plexippus, Drosophila melanogaster, Harpegnathos saltator, Nasonia vitripennis, Pediculus humanus corporis,* and *Tribolium castaneum.*

(Continued on next page)

generally cytoplasmic punctate distribution in transfected Sf9 cells (Fig. 3C) similar to that observed previously with human NSF DN constructs (34). To determine potential general effects of NSF^{E329Q}-GFP and NSF^{R385A}-GFP on the proliferation of Sf9 cells, the viability of cells expressing each construct was measured. At 12, 24, or 36 h posttransfection (p.t.), the viability of Sf9 cells transiently expressing DN NSF proteins was similar to that of cells expressing WT NSF or GFP (Fig. 3D). These data suggest that transient expression of DN NSF proteins over this short time period did not result in a measurable negative effect on the viability of Sf9 cells.

Effects of DN NSF expression or NSF knockdown on infectious AcMNPV production. To determine whether NSF is required for productive AcMNPV infection, we first used a viral complementation assay to examine AcMNPV replication in the presence of DN NSF proteins. Because not all cells become transfected and express the DN constructs in transient-transfection assays, the complementation assay ensures that productive viral replication can occur only in cells that are productively transfected and express both the DN NSF construct and WT GP64 (which complements the *gp64* knockout and permits production of infectious BV). In this assay, Sf9 cells were cotransfected with two plasmids: one expressing GP64 and another expressing either GFP, NSF, or DN NSF constructs (NSF^{E329Q}-GFP or NSF^{R385A}-GFP). At 12 h p.t., the transfected cells were infected with the *gp64* knockout virus (mCherryGUS-*gp64*^{ko}) at a multiplicity of infection (MOI) of 1 or 5. At 24 h p.i., the cell culture supernatants were harvested and the infectious virus titers were determined on a GP64-expressing cell line (Sf9^{Op1D}) that complements the *gp64* knockout virus. (Note that virus produced from the transfected cells should contain GP64 produced from the plasmid, but the virus cannot spread from cell to cell in an endpoint titration assay. Thus, the Sf9^{Op1D} cell line is used for the 50% tissue culture infectious dose [TCID$_{50}$] assay to detect virions produced in the transfection-infection assay.) As shown in Fig. 4B, the production of infectious AcMNPV is significantly reduced (>97% reduction at an MOI of 5) in the presence of either DN NSF construct, NSF^{E329Q}-GFP or NSF^{R385A}-GFP. In contrast, the expression of WT NSF had no effect on infectious virus production compared with that in cells expressing GFP. A similar result was observed when cells were infected at an MOI of 1. In these cotransfected and infected Sf9 cells, both GP64 and each of the NSF protein constructs were expressed at substantial levels (Fig. 4A). Additionally, in parallel experiments a similar reduction of infectious AcMNPV production was also observed in another lepidopteran cell line, *T. ni* High 5 cells, in the presence of DN NSF proteins (data not shown).

To extend our observations, we used a double-stranded RNA (dsRNA)-based RNAi approach to evaluate the effect of an NSF knockdown on the production of infectious AcMNPV. Sf9 cells were mock transfected or transfected with a dsRNA specific for Sf9 NSF or a dsRNA targeting a GFP control gene. Knockdown efficiencies for NSF were

TABLE 1 Continued

^{b}Qbc represents the SNARE proteins possessing one Qb-SNARE motif and one Qc-SNARE motif.
^{c}Absent from *Culex quinquefasciatus* and *Pediculus humanus corporis*.
^{d}Absent from *Acyrthosiphon pisum*.
^{e}Two orthologs of Vti1 were found in *Acyrthosiphon pisum*, *Anopheles gambiae*, *Apis mellifera*, *Culex quinquefasciatus*, *Drosophila melanogaster*, *Harpegnathos saltator*, and *Tribolium castaneum*.
^{f}Absent from *Bombyx mori* and *Danaus plexippus*.
^{g}Present only in *Apis mellifera* and *Nasonia vitripennis*.
^{h}Absent from *Harpegnathos saltator* and *Pediculus humanus corporis*.
^{i}Abbreviations: α-SNAP, α-soluble NSF attachment protein; Bet1, blocked early in transport; Bos1, Bet1 suppressor 1; Endob, endobrevin; Gos, Golgi SNARE protein (numbers indicate sizes in kDa); Lgl, lethal giant larvae; Memb, membrin; Myob, myobrevin; Nyv1, new yeast v-SNARE; Pep12, carboxypeptidase Y deficient; Sec, secretory mutant protein; Sed5, suppressor of Erd2 deletion; Sft1, suppressor of Sed5; Slt1, SNARE-like tail-anchored protein 1; Snc1/Snc2, suppressor of the null allele of CAP; SNAP, synaptosome-associated protein (numbers indicate sizes in kDa); SPO20, sporulation 20; Sro7/Sro77, suppressor of Rho3; Sso1/Sso2, supressor of Sec1; Syb, synaptobrevin; Syx, syntaxin; Tlg, T-snare affecting a late Golgi compartment; Tom, tomosyn; Ufe1, unknown function essential 1; Use1, unconventional SNARE in the ER; Vam, vacuolar morphogenesis; VAMP, vesicle-associated membrane protein; Vti1, Vps10 interacting protein; Ykt6, YKL196c-encoding protein. − or +, absence or presence, respectively, of a specific SNARE protein in yeast, human, or insects.
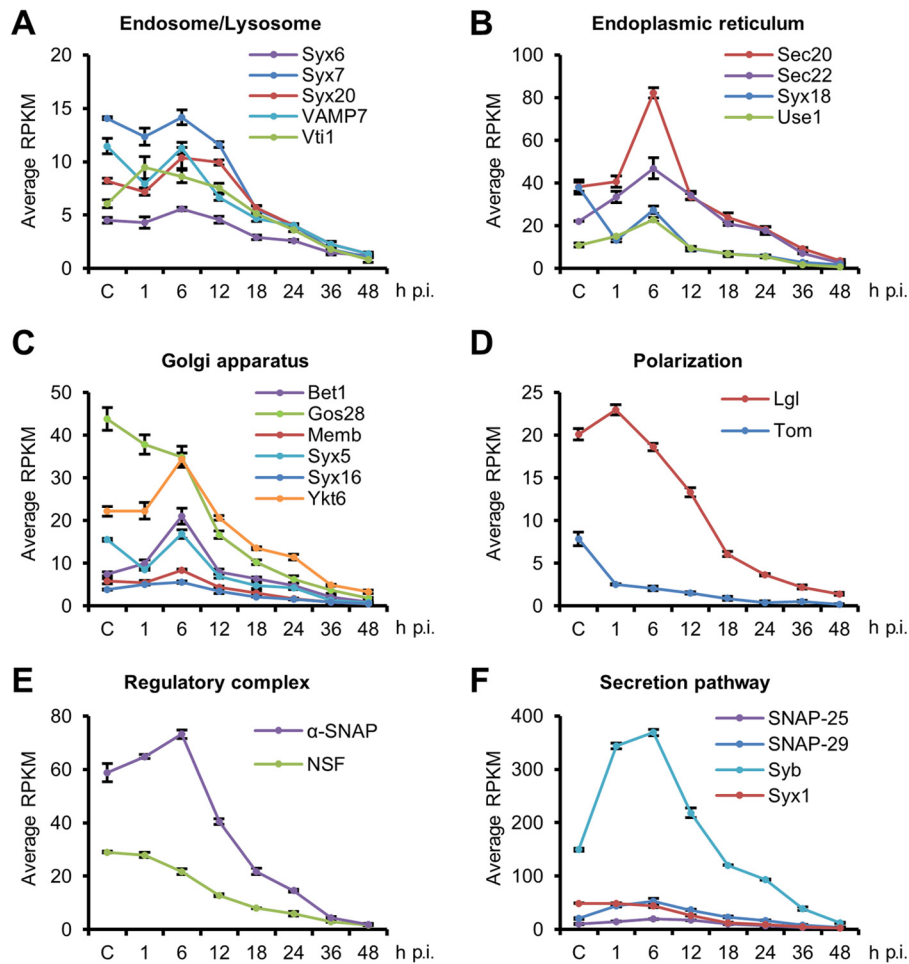
RNA-seq analysis of SNARE mRNAs in AcMNPV-infected *T.ni* cells

FIG 1 Expression profiles of the components of the cellular SNARE system before and during AcMNPV infection. Transcription data for SNARE system components were retrieved from a transcriptome analysis of AcMNPV-infected Tnms42 cells (33) and are grouped into panels A to F according to the SNARE genes that are involved in a specific pathway or complex. Measurements of transcript levels (RPKM, or reads per kilobase per million reads) from samples from control (C; uninfected) or infected cells at various time points postinfection are plotted. The RPKM values (total RPKM of <5) for γ-SNAP and Syx17 were cut off in the transcriptome analysis (33). The ortholog of Syx4 was not found in the transcriptome database. Error bars represent standard deviations from the means of three replicates. Host gene abbreviations are detailed in the footnotes to Table 1.

approximately 16.2% (24 h p.t.) and 74.6% (48 h p.t.) (Fig. 4C), and transfection with the dsRNA targeting NSF or GFP resulted in no significant change in the viability of Sf9 cells at 24, 48, and 72 h p.t. (data not shown). Similar to the results from DN NSF expression, we found that depletion of NSF also resulted in a dramatic reduction in the production of infectious AcMNPV (Fig. 4D). Together, these results suggest that functional NSF is important for the efficient replication of AcMNPV.

Effects of DN NSF on early stages of AcMNPV infection. Budded virions of AcMNPV enter host cells via clathrin-mediated endocytosis (26), which is regulated in part by the coordinated action of several SNARE proteins (Table 1) (4). The negative effects of the DN NSF and the NSF knockdown on AcMNPV BV production could result from disruption of the viral infection cycle at an early stage of infection, possibly by interfering with the transport of virions within endosomes during entry. To examine this possibility, Sf9 cells were cotransfected with two plasmids expressing GP64 and one of the following proteins: NSF-GFP, NSF^{E329Q}-GFP, NSF^{R385A}-GFP, or GFP. At 12 h p.t., the cells were infected with a *gp64* knockout virus (LacZGUS-*gp64*^{ko}) that contains
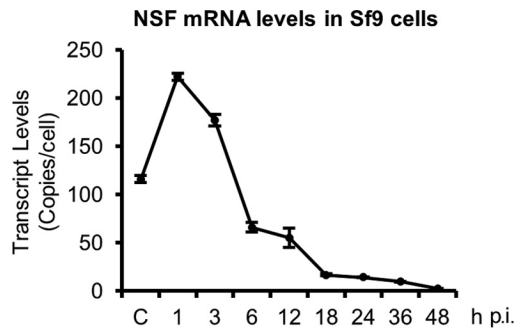
NSF mRNA levels in Sf9 cells

FIG 2 Transcript levels of NSF in AcMNPV-infected Sf9 cells. Sf9 cells were infected with wild-type AcMNPV at an MOI of 10, and total RNAs were isolated from uninfected (C; control) cells or infected cells at various time points postinfection (1 to 48 h p.i.) and transcribed into cDNA. Transcript levels of NSF were measured by quantitative real-time PCR. Error bars represent standard deviations from the means of three replicates.

two reporter genes, LacZ and β-glucuronidase (GUS), which are controlled by the AcMNPV *ie1* early/late promoter and *p6.9* late promoter, respectively. At early and later times in the infection cycle, the transfected and infected cells were lysed and relative β-galactosidase (β-Gal) and GUS activities were measured. As shown in Fig. 5A and B,
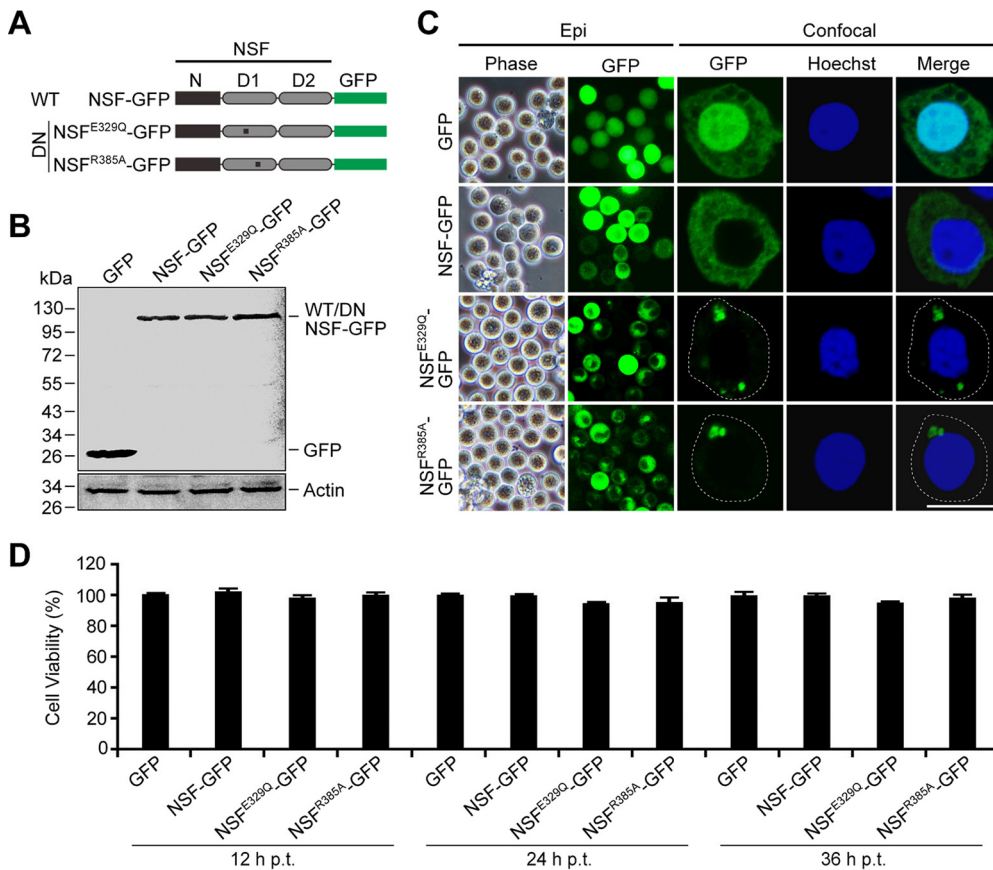

FIG 3 Transient expression of GFP-tagged wild-type (WT) and dominant-negative (DN) NSF proteins in Sf9 cells. (A) Schematic representation of domain structure and GFP fusions of WT and DN NSF constructs (NSF-GFP, NSF^{E329Q}-GFP, and NSF^{R385A}-GFP). NSF domain abbreviations: N, NSF-N domain; D1, the first ATP-binding domain; D2, the second ATP-binding domain. (B) Western blot analysis of GFP-tagged NSF proteins transiently expressed in Sf9 cells. GFP and NSF-GFP fusions were detected with an anti-GFP polyclonal antibody. The anti-β-actin blot served as a loading control. (C) Subcellular localization of WT and DN NSF-GFP fusion proteins in transfected cells by epifluorescence microscopy (Epi) (left) and confocal microscopy (right). (D) Viability of transfected cells expressing WT or DN NSF proteins was measured at various times posttransfection (12 to 36 h) using a tetrazolium-based cell viability assay as described in Materials and Methods. Error bars represent standard deviations from the means of three replicates.
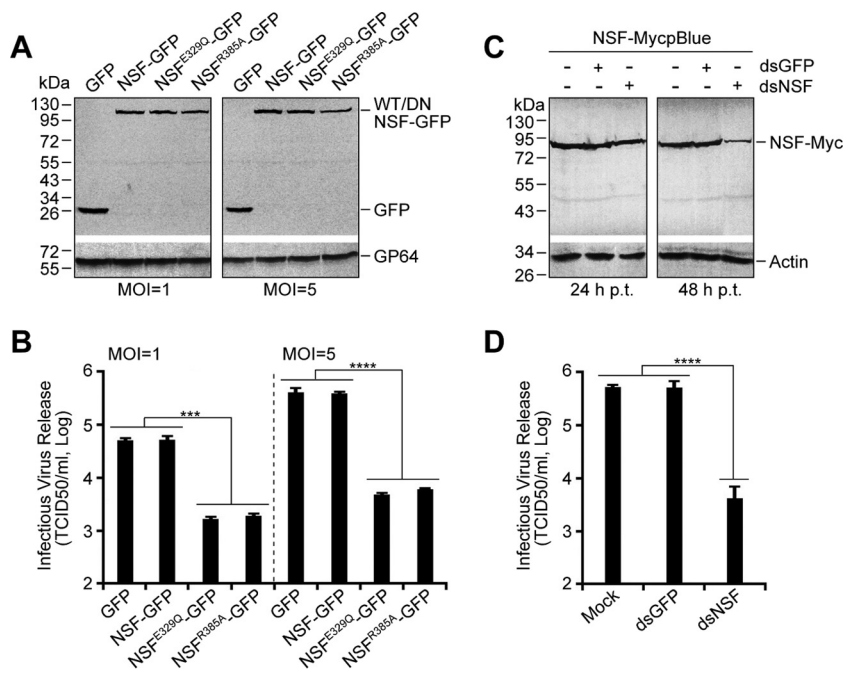
FIG 4 Effects of DN NSF expression (A and B) and NSF knockdown (C and D) on AcMNPV production. (A and B) Sf9 cells were cotransfected with two plasmids expressing GP64 and either WT NSF (NSF-GFP), DN NSF (NSF^{E329Q}-GFP or NSF^{R385A}-GFP), or GFP. (A) At 12 h p.t., cells were infected with the *gp64*-knockout virus (mCherryGUS-*gp64*^{ko}) at an MOI of 1 or 5. At 24 h p.i., expression of GP64 and GFP-tagged WT and DN NSF in transfected-infected cells was confirmed by Western blotting of cell lysates. (B) Effects of DN NSF proteins were analyzed by measurements of the titers of infectious BV released from transfected-infected cells. (C) Sf9 cells were transfected with an NSF-MycpBlue plasmid or cotransfected with an NSF-MycpBlue plasmid and the dsRNA targeting NSF or GFP (dsNSF and dsGFP). At 24 and 48 h p.t., the transfected cells were collected and the expression of Myc-tagged NSF was detected by Western blotting with an anti-Myc polyclonal antibody. The anti-β-actin blot served as a loading control. (D) Sf9 cells were mock transfected (Mock) or transfected with the dsRNA targeting NSF or GFP (dsNSF and dsGFP). At 48 h p.t., the transfected cells were infected with wild-type AcMNPV at an MOI of 5. At 24 h p.i., the cell culture supernatants were collected and the virus titers were determined by TCID$_{50}$ assays. Error bars represent standard deviations from the means of three replicates. ***, $P < 0.0005$; ****, $P < 0.00005$ (by unpaired *t* test).

the activities of both β-Gal and GUS were similar in cells expressing control protein GFP or NSF-GFP. However, in the presence of the two DN NSF proteins (NSF$^{E329\text{-GFP}}$ or NSF^{R385A}-GFP), both β-Gal and GUS activities were significantly reduced compared with that of the controls (Fig. 5A and B). In addition, viral genomic DNA was isolated from transfected-infected cells (under the same conditions), and viral genomic DNA replication efficiency was measured by quantitative real-time PCR detection of genomic DNA. The results showed that the transient expression of DN NSF proteins (NSF^{E329}-GFP or NSF^{R385A}-GFP) resulted in a significantly reduced level of viral genomic DNA (Fig. 5C). Because early and late gene expression and viral DNA replication were all reduced, these results suggest that the presence of DN NSF proteins inhibits viral infection at a step prior to early gene expression, possibly inhibiting trafficking of the virion entering from the cell surface to the nucleus.

Effects of DN NSF on internalization and transport of AcMNPV BV during entry. Several SNARE proteins and NSF (which regulates their function) play important roles in endocytosis by mediating vesicle fusion (4, 35). To examine whether viral entry by endocytosis involved SNARE-mediated fusion events, we examined mCherry-tagged BV entry in the presence of WT or DN NSF proteins. We first transfected Sf9 cells with a plasmid expressing either WT NSF, DN NSF, or GFP. After a 12-h period of expression, cells were incubated with mCherry-labeled AcMNPV virions (AcMNPV-3mC) at 4°C for 60 min to permit virus adsorption at the cell surface. After removing the viral inoculum and washing the cells twice with cold medium, the temperature was raised to 27°C and cells were incubated for 60 min. Internalized virus was quantified by qRT-PCR mea-
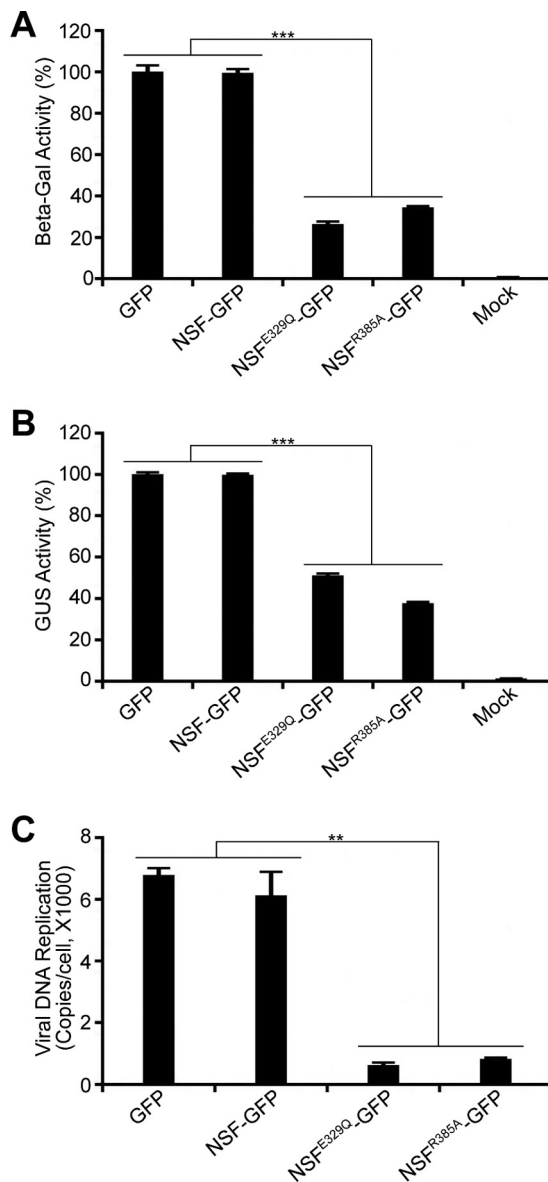
FIG 5 Effects of DN NSF on early stages of AcMNPV infection. The effects of DN NSF proteins on early and late viral gene expression and viral DNA replication were examined. Sf9 cells were cotransfected with two plasmids expressing GP64 and WT NSF (NSF-GFP), DN NSF (NSF^{E329Q}-GFP or NSF^{R385A}-GFP), or GFP. At 12 h p.t., the transfected cells were infected with a *gp64* knockout virus (LacZGUS-*gp64*^{ko}). (A) Early gene expression was monitored by analyzing AcMNPV *ie1* early/late promoter-driven β-Gal activity at 6 h p.i. (B) Late-phase gene expression was monitored by analyzing AcMNPV *p6.9* late promoter-driven GUS activity at 24 h p.i. (C) Viral DNA replication was monitored by quantitative real-time PCR analysis of viral genomic DNA extracted from transfected-infected cells at 24 h p.i. Error bars represent standard deviations from the means of three replicates. **, $P < 0.005$; ***, $P < 0.0005$ (by unpaired *t* test).

surements of viral genomic DNA. Internalized viral DNA was dramatically reduced in cells expressing DN NSF proteins (61.8% and 65.0% reduction in NSF^{E329Q}-GFP- and NSF^{R385A}-GFP-expressing cells, respectively) compared with cells expressing the WT NSF protein or the control GFP (Fig. 6A). In addition to qRT-PCR, the transport of virions was also analyzed by confocal microscopy (Fig. 6B). In control cells expressing WT NSF or GFP, the mCherry-labeled nucleocapsids were observed as small but discrete foci of fluorescence distributed more evenly throughout the cytoplasm, and some were observed within the nucleus. In contrast, the mCherry-labeled nucleocapsids in cells expressing DN NSF proteins (NSF^{E329Q}-GFP and NSF^{R385A}-GFP) were observed aggregated in the cytoplasm in discrete foci which likely represent endosomes. Interestingly,
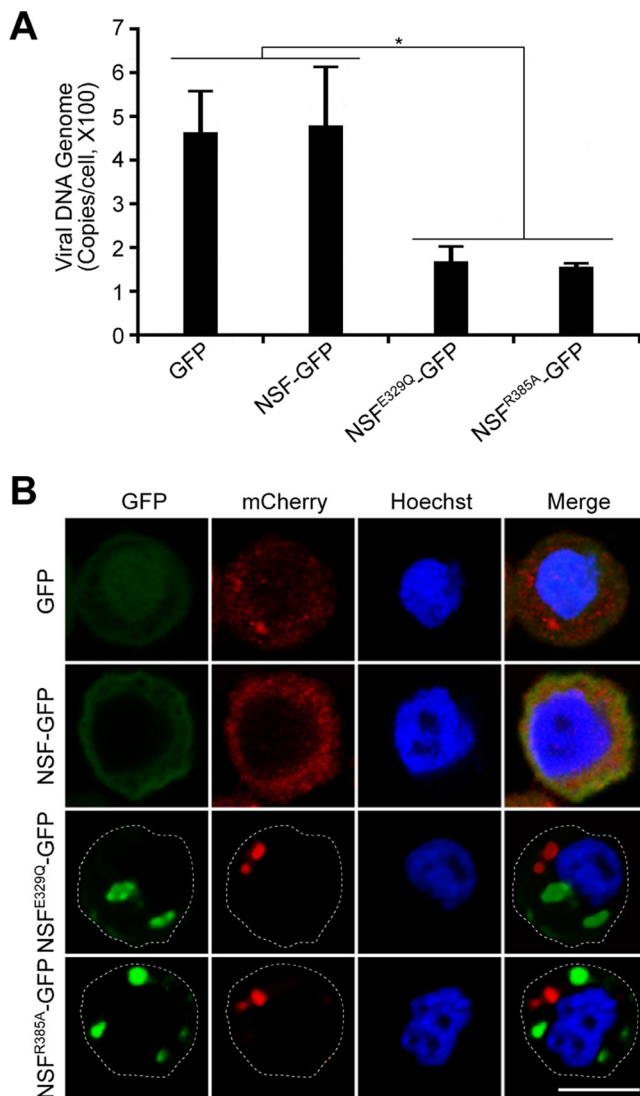
FIG 6 Effects of DN NSF on AcMNPV entry. Sf9 cells were transfected with plasmids expressing either WT NSF (NSF-GFP), DN NSF (NSF^{E329Q}-GFP or NSF^{R385A}-GFP), or GFP. At 12 h p.t., the cells were infected at 4°C for 60 min with an AcMNPV containing mCherry-tagged VP39 capsid protein. After raising the culture temperature to 27°C for 60 min, the internalization and transport of entering virions were analyzed by quantitative real-time PCR analysis of viral DNA from cell lysates (A) and by confocal microscopic detection of mCherry-tagged capsids (B). Error bars represent standard deviations from the means of three replicates. Scale bar, 10 μm. *, $P < 0.05$ (by unpaired t test).

the aggregated mCherry-tagged nucleocapsids were not colocalized with GFP-tagged DN NSF proteins (Fig. 6B, lower, GFP versus mCherry). Thus, while quantitative PCR results suggested that binding and entry were affected by DN NSF expression, confocal microscopy showed that transport of AcMNPV nucleocapsids was also disrupted. Overall, these data suggest that NSF is required for efficient internalization and intracellular transport of AcMNPV BV during entry.

Is NSF required for efficient egress of infectious AcMNPV? In the studies described above, we found that expression of DN NSF proteins in Sf9 cells led to inefficient internalization and transport of AcMNPV BV. Therefore, to study the role of NSF in virion egress and to circumvent the negative effects on virus entry, we initiated infections by transfecting Sf9 cells with AcMNPV bacmid DNA. Each AcMNPV bacmid DNA expressed a WT or DN NSF protein (tagged with GFP) plus a reporter GUS protein. NSF constructs were expressed from the viral genome under the control of the AcMNPV *ie1* early/late promoter, and the GUS reporter gene was expressed from the *p6.9* late
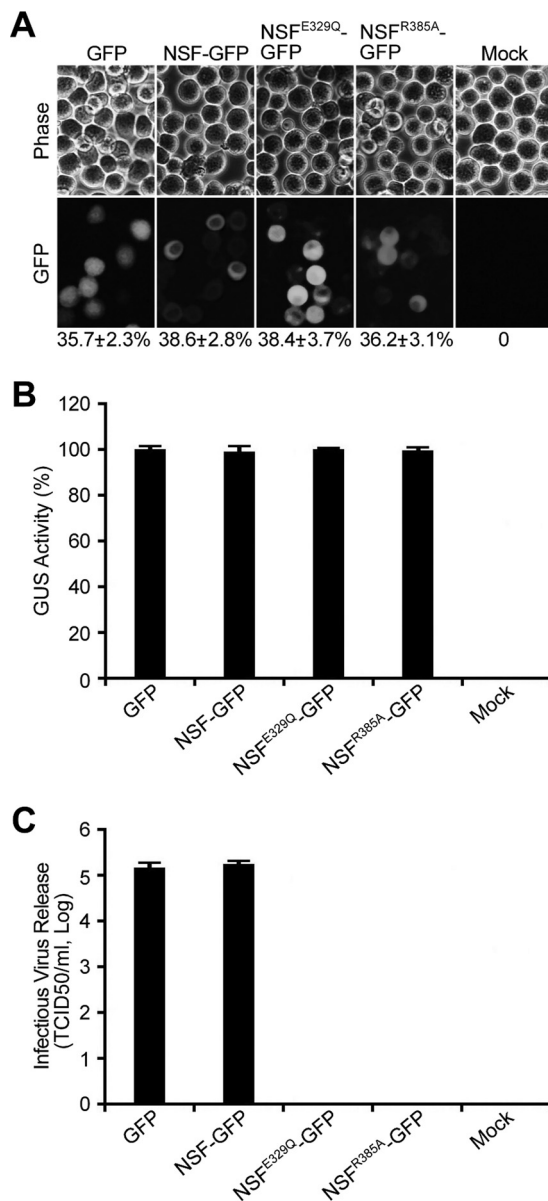
FIG 7 Effects of DN NSF proteins on production of infectious budded virions. Sf9 cells were transfected with bacmid DNA expressing either WT NSF (NSF-GFP), DN NSF (NSF^{E329Q}-GFP or NSF^{R385A}-GFP), or GFP. (A) Transfection activity was monitored by analysis of GFP-positive cells. Percentages of GFP-positive cells at 24 h p.t. are indicated below each micrograph of GFP epifluorescence. (B) Late-phase gene expression was monitored by analysis of GUS activity from a *p6.9* late promoter-driven GUS gene at 24 h p.t. (C) Production of infectious BV was measured by TCID$_{50}$ assay of cell culture supernatants collected at 24 h p.t. Error bars represent the standard deviations from the means of three replicates.

promoter. Thus, DN-NSF proteins were expressed in the early phase of infection prior to egress, which occurs during the late phase after assembly of progeny nucleocapsids. Because NSF is a homohexamer (9) that is continually assembling and disassembling, DN NSF expressed early should inactivate the function of preexisting wild-type NSF. At 24 h posttransfection, GFP-positive cells were scored to evaluate transfection efficiency and expression of the NSF-GFP fusions. In parallel, late promoter-driven GUS activity was measured to monitor progression of the viral infection. As shown in Fig. 7, the percentage of GFP-positive cells from transfections with different bacmids (GFPBac, NSF-GFPBac, NSF^{E329Q}-GFPBac, and NSF^{R385A}-GFPBac) varied from 35.7% to 38.4% (Fig. 7A). Also, relative GUS activities measured from the transfected cell lysates from cells transfected with the same bacmid DNAs were also at similar levels (Fig. 7B). These

results indicate that, in cells transfected with the different bacmids (expressing GFP, NSF-GFP, or DN NSF constructs), transfection efficiencies were approximately equivalent, and in all cases virus infection progressed into the late phase. Virus titers in supernatants from cells expressing NSF-GFP or the control GFP were both approximately 2.5×10^5 TCID$_{50}$/ml. In contrast, no infectious AcMNPV BV was detected in supernatants (24 h p.t.) from cells expressing DN NSF construct NSF^{E329Q}-GFP or NSF^{R385A}-GFP (Fig. 7C). Thus, these data suggest that NSF is required for the egress and production of infectious AcMNPV BV.

Is cell surface expression of functional GP64 dependent on NSF? Since the viral envelope glycoprotein GP64 is necessary for production of infectious BV (36) and is trafficked through the secretary pathway, the SNARE system may be important for GP64 trafficking. Therefore, we asked whether DN NSF proteins affected expression, transport, and/or cell surface localization of GP64 in the context of a viral infection. To address this question, we transfected Sf9 cells with AcMNPV bacmid DNA expressing either WT NSF or DN NSF proteins (both tagged with GFP) as described above. At 24 h p.t., the expression of GP64 in these bacmid-transfected Sf9 cells was examined by Western blotting under reducing and nonreducing conditions for SDS-PAGE. Under nonreducing conditions, GP64 is found as disulfide-linked trimers of GP64 monomers. Two forms of GP64 trimers (known as Trimer I and Trimer II) are typically observed in infected cells (37–39). These typical forms of GP64 were detected in cells expressing DN NSF proteins (NSF^{E329Q}-GFP or NSF^{R385A}-GFP) and in cells expressing control proteins WT NSF-GFP and GFP (Fig. 8A). The intensities of the trimeric and monomeric GP64 bands were similar for all bacmid-transfected cells, suggesting that the DN NSF proteins did not substantially alter the expression, stability, or oligomerization of GP64. Cell surface-localized GP64 was examined by cellular enzyme-linked immunosorbent assay (cELISA) with the AcV5 antibody and by immunofluorescence analysis with the monoclonal antibody (MAb) AcV1, which recognizes the native neutral pH conformation of GP64 (40) (Fig. 8B and C). In cells expressing DN NSF proteins, the cell surface levels of GP64 were reduced to approximately 40% of that from cells expressing WT NSF or GFP (Fig. 8B). Although GP64 cell surface levels were significantly reduced in the presence of DN NSF, the recognition of surface-localized GP64 by MAb AcV1 indicates that GP64 is in the native conformation. To determine whether the presence of DN NSF proteins affected the fusion activity of GP64 expressed in those cells, we measured fusion activity of GP64 on cells transfected with bacmids expressing WT or DN NSF proteins. Because cell surface levels of GP64 varied between the cells expressing WT and DN NSF proteins and surface GP64 levels may affect the detection of membrane fusion activity, we initially generated a standard curve of cell surface levels of GP64 by transfecting Sf9 cells with decreasing quantities of the bacmid that expresses wild-type NSF and performed cELISA analysis (Fig. 8B). A parallel standard curve of pH-triggered membrane fusion levels was generated by transfecting cells with decreasing quantities of the same bacmid (Fig. 8D, NSF-GFP) and measuring fusion activity as percentages of cells in syncytial masses. Comparisons of GP64-mediated fusion activity in cells expressing DN NSF constructs (NSF^{E329Q}-GFP and NSF^{R385A}-GFP) with fusion from WT NSF-expressing cells in which GP64 was present at the same levels show that there was no apparent effect on GP64-mediated fusion efficiency in the presence of DN NSF proteins (Fig. 8B and D). Thus, while expression of the DN NSF proteins caused a moderate decrease in surface levels of GP64, there was no effect on the function of the surface-localized protein.

We also examined infectious BV produced from cells transfected with bacmids expressing WT or DN NSF proteins. When cells were transfected with the bacmid expressing WT NSF (NSF-GFPBac; 2.5 μg) or expressing a control GFP, we detected infectious BV titers of approximately 1.5×10^5 TCID$_{50}$/ml. However, in supernatants from cells transfected with DN NSF constructs NSF^{E329Q}-GFPBac and NSF^{R385A}-GFPBac, no infectious BV was detected (Fig. 8E). Thus, while NSF may play a minor role in intracellular transport and cell surface localization of GP64, the defect in infectious
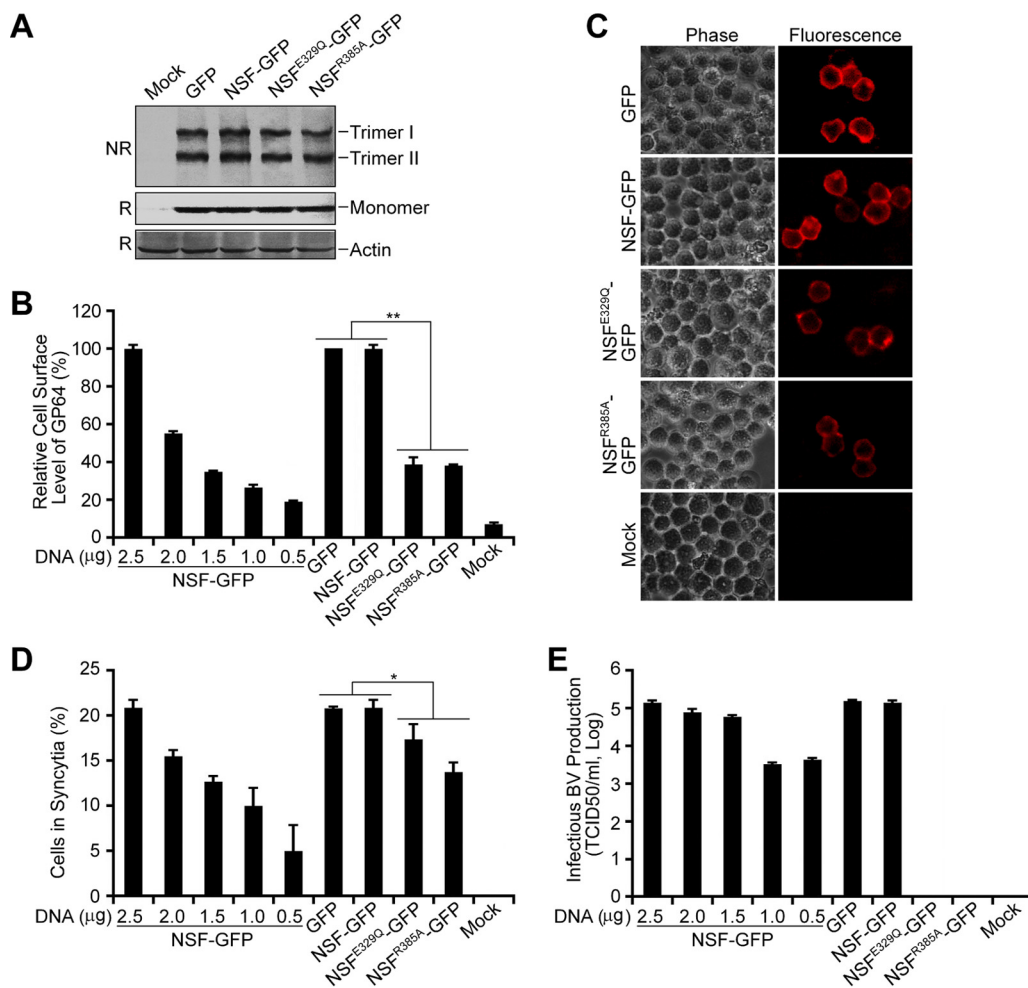
FIG 8 Effects of DN NSF on cell surface levels of GP64. Sf9 cells were transfected with 2.5 μg bacmid DNA expressing GFP-tagged NSF proteins (WT or DN) or GFP. To generate a standard curve for GP64 surface levels and for cell-cell fusion analysis, cells were transfected with 0.5 to 2.5 μg bacmid DNA expressing GFP-tagged WT NSF. At 24 h p.t., the expression, cell surface localization, and fusion activity of GP64 and infectious virus production were analyzed. (A) Western blot analysis of the expression and oligomerization of GP64 on reducing (R) and nonreducing (NR) gels. The anti-β-actin blot served as a loading control. (B and C) The transfected cells were fixed and the cell surface localization of GP64 was detected by cELISA using AcV5 antibody (B) or by indirect immunofluorescence using AcV1 antibody (C). (D) Transfected cells were treated with PBS at pH 5.0 to induce GP64-mediated cell-cell syncytium formation. The percentages of nuclei in syncytia (defined as more than five nuclei per syncytium) in five fields were calculated. (E) Infectious BV production from transfected cells expressing WT or DN NSF proteins or GFP was determined by TCID$_{50}$ assays. Error bars represent the standard deviations from the means of three replicates. *, $P < 0.05$; **, $P < 0.005$ (by unpaired t test).

AcMNPV BV production in the presence of DN NSF proteins was dramatic and was not explained by the modestly lower cell surface levels of GP64.

Effects of DN NSF on nucleocapsid egress from the nuclear membrane. To examine the stage of virion egress that was affected by DN NSF proteins, we first used transmission electron microscopy (TEM) of bacmid-transfected cells to compare the transport of nucleocapsids in control cells with that in cells expressing DN NSF proteins. In cells expressing WT NSF-GFP, a typical AcMNPV infection is observed. We observed the typical presence of an electron-dense VS in the nucleus, rod-shaped nucleocapsids at the edges of the VS, intranuclear microvesicles (IM), and nucleocapsids budding from the nuclear membrane (NM) and from the plasma membrane (PM) (Fig. 9A to D). Cells expressing DN NSF proteins (NSF^{E329Q}-GFP and NSF^{R385A}-GFP) also showed the VS, abundant rod-shaped nucleocapsids, numerous IM, and nucleocapsids associated with IM in the nuclei (Fig. 9E, F, I, and J). However, no progeny nucleocapsids were observed budding from the plasma membrane (Fig. 9G and K). Interestingly, in cells expressing
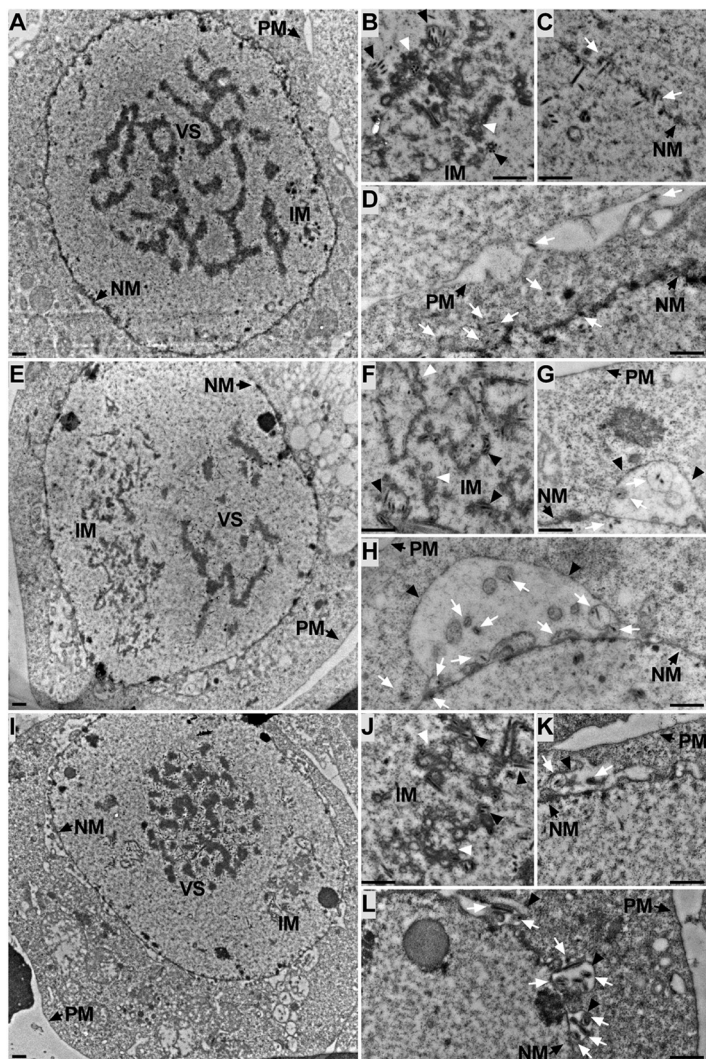
FIG 9 TEM analysis of AcMNPV-infected Sf9 cells expressing WT or DN NSF proteins. Sf9 cells were transfected with AcMNPV bacmids expressing either wild-type NSF (A to D) or dominant-negative NSF protein NSF^{E329Q}-GFP (E to H) or NSF^{R385A}-GFP (I to L). At 48 h posttransfection, the bacmid-transfected cells were fixed and analyzed by transmission electronic microscopy. Electron-dense virogenic stroma (VS) and intranuclear microvesicles (IM) were observed in cells expressing both WT NSF and DN NSF (A versus E or I). White and black triangles show IM and nucleocapsids associated with the membranous vesicular structures, respectively (B versus F versus J). Progeny nucleocapsids (white arrows) appear to be budding into the nuclear membrane (NM; black arrows) (C) and free in the cytoplasm (D) in cells expressing WT NSF. In contrast, nucleocapsids (white arrows) were found primarily in large perinuclear spaces or vesicular structures (black triangles) associated with the nuclear membrane in cells expressing DN NSF (G, H, K, and L). PM, plasma membrane. Scale bar, 500 nm.

DN NSF proteins, some progeny nucleocapsids were observed budding through the inner nuclear membrane (INM), but the INM-enclosed nucleocapsids appeared to be trapped within a perinuclear space formed by the inner nuclear membrane and the deformed outer nuclear membrane (Fig. 9G, H, K, and L). Combined with the absence of BV production in the presence of DN NSF, these results suggest that functional NSF could be important, directly or indirectly, for transit of progeny nucleocapsids across the nuclear membrane.

Association of NSF with viral proteins. Viruses in the family *Baculoviridae* contain a set of about 37 core genes that are conserved in most or all sequenced baculovirus genomes (22). Recent studies reported that some of these baculovirus core proteins and some of the highly conserved viral proteins are important for the release of progeny nucleocapsids from nuclei (41–48). These proteins include Ac11, Ac76, Ac78,
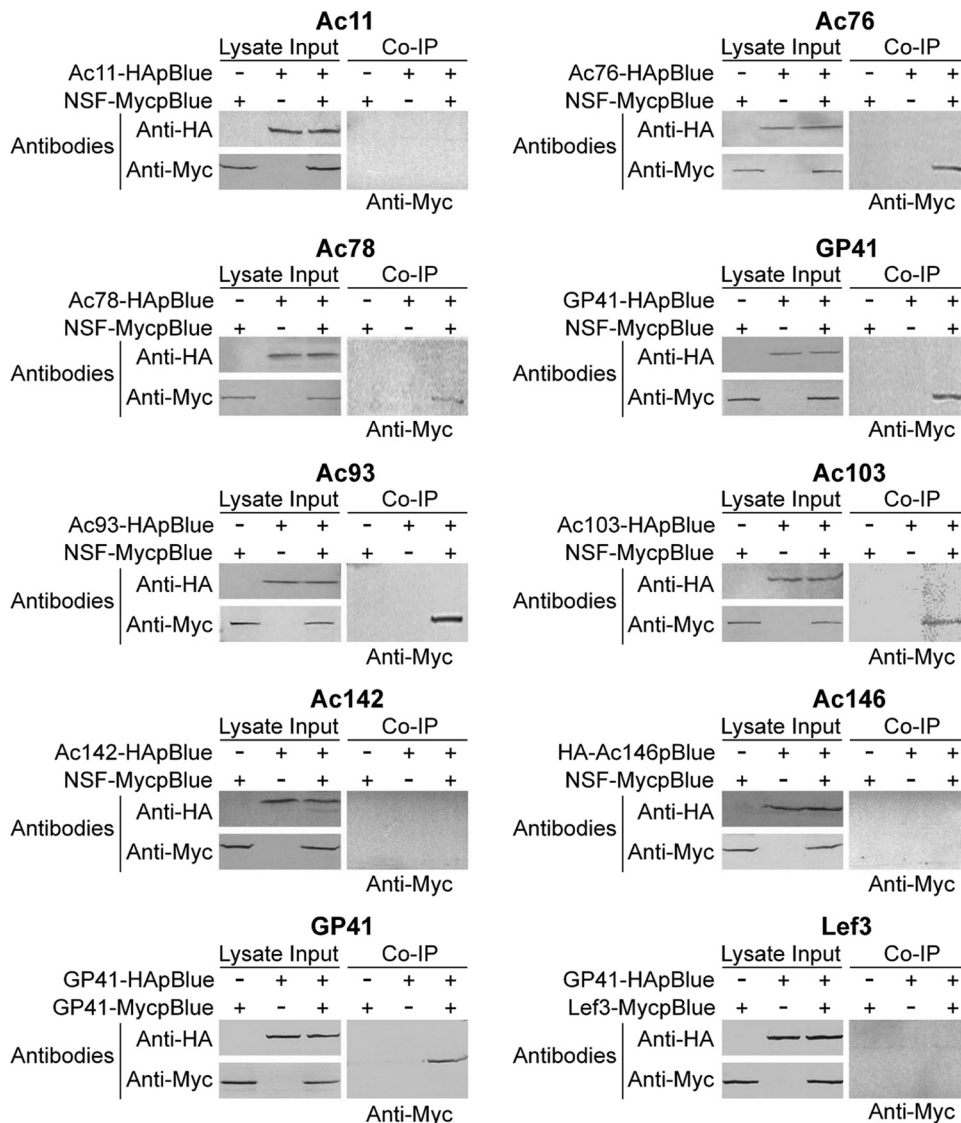
FIG 10 Coimmunoprecipitation analysis of NSF and AcMNPV proteins. Sf9 cells were transfected or cotransfected with two plasmids separately expressing NSF-Myc and an HA-tagged viral protein. At 36 h p.t., the cells were lysed and the proteins were immunoprecipitated with anti-HA monoclonal antibody and protein G agarose. The precipitates (co-IP) were detected on Western blots with an anti-Myc polyclonal antibody (right panel in each group). The cell lysates (lysate input) were also examined on Western blots with an anti-HA monoclonal antibody (top) or an anti-Myc polyclonal antibody (bottom).

Ac80 (GP41), Ac93, Ac103, Ac142, and Ac146. A similar defect in infectious AcMNPV production, combined with the aberrant nuclear structures observed at the nuclear membrane (both caused by DN NSF proteins), suggests that NSF also are involved in egress of nucleocapsids from the nucleus, perhaps associating with some of the above-described baculovirus highly conserved or core proteins. To test this hypothesis, an immunoprecipitation assay was used to examine the potential association between NSF and each of the above-described viral proteins. We selected AcMNPV GP41 and Lef3 as control proteins, as it was previously demonstrated that GP41 interacts with itself but does not interact with Lef3 (49). Sf9 cells were cotransfected with two plasmids: one expressing a hemagglutinin (HA)-tagged viral protein and another expressing NSF-Myc. At 36 h p.t., the cells were lysed and proteins were immunoprecipitated with an anti-HA MAb. Expression of the HA-tagged and Myc-tagged proteins was confirmed by Western blotting using appropriate antibodies (Fig. 10). Of the 8 viral proteins examined, we found that 5 coimmunoprecipitated (co-IP) NSF, suggesting that
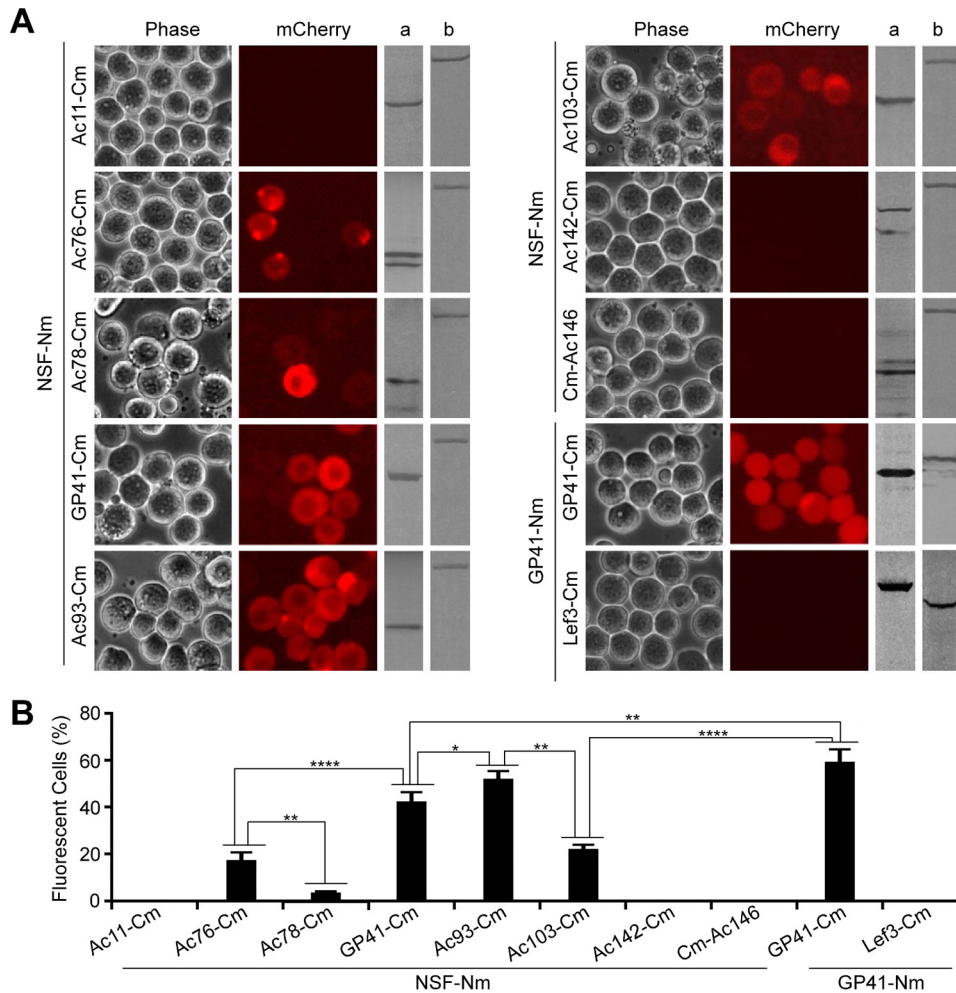
FIG 11 BiFC analysis of NSF and AcMNPV protein associations. Sf9 cells were cotransfected with a pair of BiFC plasmids, one expressing NSF-HA-Nm (NSF-Nm) and the other expressing a viral protein fused with Myc-Cm (e.g., Ac11-Cm or Cm-Ac146). As controls, cells were transfected with plasmid pairs expressing GP41-HA-Nm and GP41-Myc-Cm or GP41-HA-Nm and Lef3-Myc-Cm. At 36 h p.t., cells were examined for fluorescence complementation by epifluorescence microscopy (A), and the percentage of mCherry-positive cells in five fields was calculated (B). The expression of each construct in cotransfected cells was confirmed by Western blotting with anti-Myc antibody (A, a) or anti-HA antibody (A, b). Error bars represent the standard deviations from the means of three replicates. *, $P < 0.05$; **, $P < 0.005$; ****, $P < 0.00005$ (by unpaired t test).

viral proteins Ac76, Ac78, GP41, Ac93, and Ac103 either interact with NSF or are found in a complex that includes NSF (Fig. 10).

To extend the results from coimmunoprecipitation studies, we further examined the possible associations of NSF and viral proteins using a bimolecular fluorescence complementation assay (BiFC) in living cells. Sf9 cells were cotransfected with two plasmids, separately expressing NSF and one of the viral proteins, with each as a fusion with the N- or C-terminal domain of mCherry (referred to as Nm or Cm, respectively). Initially, to verify the specificity of the mCherry-based BiFC system, we also selected AcMNPV GP41 and Lef3 as candidate bait and prey proteins. By coexpressing GP41-HA-Nm with either GP41-Myc-Cm or Lef3-Myc-Cm (Nm and Cm represent N- and C-terminal fragments of mCherry, respectively), we observed mCherry fluorescence complementation in approximately 50% of the cells cotransfected with GP41-HA-Nm and GP41-Myc-Cm plasmids (Fig. 11A, lower right). In contrast, fluorescence was not detected in cells coexpressing GP41-HA-Nm and Lef3-Myc-Cm, even though both of the fusion proteins were expressed (Fig. 11A, lower right). In cells coexpressing NSF-HA-Nm in combination with Cm-tagged viral proteins, BiFC fluorescence was observed between combinations
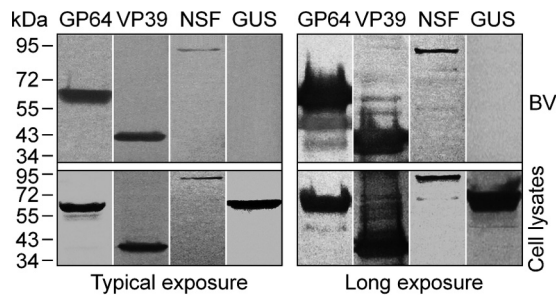
FIG 12 Detection of NSF in budded virions of AcMNPV. Sf9 cells were transfected with bacmid NSF-MycBac, which expresses a Myc-tagged WT NSF protein. At 72 h p.t., cell supernatants were collected and the budded virions were purified by sucrose density gradient centrifugation. The transfected cells and the purified virions were analyzed on Western blots using anti-GP64, anti-VP39, anti-Myc, and anti-GUS antibodies. BV, budded virions. Typical and long (left and right, respectively) exposures of Western blots are shown, illustrating the presence of NSF at low quantities in BV preparations.

of NSF and Ac76, Ac78, GP41, Ac93, or Ac103, the same 5 proteins identified in co-IP studies. The percentage of fluorescent cells was highest (40 to 50%) in cells coexpressing NSF-HA-Nm with GP41-Myc-Cm or Ac93-Myc-Cm (Fig. 11B). Lower percentages of fluorescent cells (5 to 18%) were observed when NSF-HA-Nm was coexpressed with Ac76-Myc-Cm, Ac78-Myc-Cm, or Ac103-Myc-Cm. While Western blot analysis showed that all of the fusion proteins were expressed in cotransfected Sf9 cells, we observed no BiFC fluorescence in cells coexpressing NSF-HA-Nm with constructs Ac11-Myc-Cm, Ac142-Myc-Cm, and Cm-Myc-Ac146. (Note that two different size bands were detected in Western blots for Ac76-Myc-Cm and Cm-Myc-Ac146, and this phenomenon has been described previously [44, 45]). Similar BiFC fluorescence results were observed by reciprocal protein fusions of Nm fused to viral proteins and Cm fused with NSF (data not shown). Thus, our initial co-IP results were confirmed in BiFC experiments in which associations occur and are detected within live cells. While these data suggest protein-protein interactions, BiFC interactions can occur at distances of up to 7 nm and therefore are not definitive evidence of direct protein-protein interactions. Thus, combined with effects of DN NSF on virus egress, these co-IP and BiFC studies suggest that the baculovirus conserved (core) structural proteins (Ac76, Ac78, GP41, Ac93, and Ac103) are closely associated with NSF, and complexes of these proteins with cellular NSF may be involved in AcMNPV egress.

Association of NSF with AcMNPV BV. NSF is important for efficient entry and egress of AcMNPV BV and is closely associated with conserved viral structural proteins. These findings suggested that NSF is assembled into BV during the maturation process. To examine this possibility, Sf9 cells were transfected with AcMNPV bacmid DNA expressing c-Myc-tagged NSF and a GUS reporter (NSF-MycBac), and BV preparations were probed for the presence of NSF-Myc by Western blotting. While a negative control (GUS) was not detected in BV, Myc-tagged NSF was detected in both purified BV and cell lysates (Fig. 12, NSF). Positive controls GP64 and VP39 were also detected in both cell lysates and BV. A role for NSF in BV is not known, but it is possible that NSF in the virion plays a role during entry or that NSF is assembled into the BV fortuitously during virion egress.

DISCUSSION

The infection of insect cells by baculoviruses involves a complex interplay between cell and virus (32, 33, 50–52). Analysis of transcriptome data from AcMNPV-infected *Trichoplusia ni* Tmns42 cells (33) showed that early in the infection, many host genes are upregulated immediately following virus inoculation, and among these are a number of SNARE-encoding genes (Fig. 1, Table 1). SNARE proteins function as protein complexes that mediate fusion between intracellular transport vesicles and membrane-bound compartments, and they are important in endocytosis, endoplasmic reticulum (ER) and Golgi trafficking, and the secretary pathway (1). The activity of the SNARE

system is regulated by a complex that is formed by NSF and α-SNAP (9). In AcMNPV-infected Tnms42 cells, α-SNAP and a number of SNARE-related genes are slightly to moderately upregulated early after infection and then decline as infection progresses (Fig. 1). The levels of NSF transcripts are not increased but decrease gradually after infection. For comparison, we examined the transcript levels of NSF in AcMNPV-infected Sf9 cells and found that at 1 and 3 h p.i. NSF transcripts were moderately elevated but had decreased by 6 h p.i. (Fig. 2). It is unclear whether these cell line differences are significant. However, because of their critical roles in cells, we asked whether they also are important for productive viral infection. During entry, AcMNPV nucleocapsids typically are trafficked to the nucleus within approximately 1 h after inoculation (29, 53). During this time, the cellular SNARE system components should be fully intact and functional. We found that general disruption of the SNARE machinery in insect cells (by overexpressing DN NSF or by downregulating NSF using RNAi) resulted in dramatically reduced infectious AcMNPV production. To understand how viral replication was constrained, we examined the roles of NSF in both entry and egress.

Budded virions of AcMNPV enter host cells via clathrin-mediated endocytosis (26, 54). Endosomes are then trafficked within the cell, and during this process they are gradually acidified. The decreasing pH within endosomes triggers a conformational change in the major viral envelope glycoprotein (GP64) which mediates membrane fusion and release of the nucleocapsid into the cytosol (28). Prior studies (55) measuring AcMNPV virion internalization from the cell surface and transit time within the endosome estimated that virus entry required approximately 12.5 min from binding until entry into the endosome and another approximately 12.5 min before virions become insensitive to an inhibitor of endosome acidification, indicating release from the endosome. After endosome release, nucleocapsids are transported to the nucleus by a mechanism that involves actin polymerization (29). Using DN NSF constructs, we found that virus entry required a functional SNARE system. We initially observed that expression of DN NSF resulted in reduced reporter gene expression, reduced viral DNA replication, and lower production of infectious progeny virus (Fig. 4 and 5). Because those results were consistent with an entry or early phase defect, we examined virion entry more directly by tracking the entry of virions containing mCherry-tagged nucleocapsids. In the presence of DN NSF, we found that mCherry-labeled nucleocapsids were aggregated in the cytoplasm, indicating that they were not efficiently transported to the nucleus and perhaps were trapped within endosomes (Fig. 6B).

In mammalian cells, the homotypic fusion of early endosomes is driven by a SNARE complex consisting of an R-SNARE (VAMP4) and Q-SNAREs (Syx6, Syx13, and Vti1a). Late endosome or endosome-lysosome fusion is mediated by SNARE complexes consisting of three Q-SNAREs (Syx7, Syx8, and Vti1b) and one R-SNARE (VAMP7 or VAMP8) (1). (Note that we did not find orthologs of Syx13 or VAMP8 in sequenced insect genomes, and orthologs of Syx8, VAMP4, and Vti1b were not found in Lepidoptera insect genomes [Table 1]). AcMNPV virion entry by receptor-mediated endocytosis may require the function of these or other SNARE complexes. Analysis of gene expression of SNARE components in AcMNPV-infected *T. ni* cells shows that the components of these SNARE complexes are either initially upregulated during infection or are maintained at constant levels for the first few hours of infection (Fig. 1). Because AcMNPV BV entry appears to be relatively rapid, preexisting levels of SNARE complex proteins are likely to be sufficient for BV entry, and changes associated with infection may represent either cellular defensive reactions to infection or virus-induced changes associated with requirements for SNARE complexes at later stages in the infection cycle. The importance of SNARE proteins in entry for some other viruses was demonstrated for certain negative-stranded RNA viruses, including influenza virus and VSV (20). For influenza virus and VSV, VAMP8 (which forms the SNARE complex with endosomal Q-SNAREs Syx7, Syx8, and Vti1b) is recruited to the virus-containing endosome and promotes virus entry (20). Presently, the series of events associated with trafficking of baculovirus BV through endosomes during entry has received little attention, and further studies of the requirements and/or interactions

of cellular factors such as the SNARE complex proteins should provide new and valuable mechanistic details on baculovirus entry.

Substantial budding of infectious AcMNPV BV can be detected from infected cells by 24 h p.i. (22). Early TEM studies showed that progeny nucleocapsids that assembled in the nucleus appeared to exit the nucleus by budding through the nuclear membrane (31). Enveloped nucleocapsids (often with double membranes presumably derived from inner and outer nuclear membranes) were observed in the cytoplasm. The observation of free nucleocapsids in the cytoplasm suggested that these nucleocapsids were deenveloped by an unknown mechanism prior to transport to the plasma membrane, where free nucleocapsids bud through the plasma membrane (31, 56). Recent studies (57) indicate that nucleocapsid trafficking during egress requires functional kinesin, suggesting that either enveloped or free nucleocapsids move along microtubules during egress. Actin may also be involved in nucleocapsid egress, as actin has been shown to be involved in nucleocapsid trafficking during entry (29). Expression of DN NSF caused a modest but significant reduction in surface levels of GP64 (Fig. 8B) and a dramatic reduction in infectious BV production (Fig. 8E). However, GP64 produced in the presence of DN NSF was oligomerized and transported to the cell surface and appeared fully functional as a fusion protein (Fig. 8), suggesting that the modest effects of DN NSF proteins on GP64 trafficking do not explain the defect in infectious AcMNPV production. We therefore used TEM to further examine the effects of DN NSF proteins on egress. When examining the nuclear membranes in the late phase of infection, we found that the presence of DN NSF proteins resulted in large perinuclear spaces formed by the INM and a deformed outer nuclear membrane (Fig. 9G, H, K, and L). Interestingly, it is known that the SNARE system participates in nuclear membrane remodeling in *Xenopus laevis* eggs (58). The observation that AcMNPV nucleocapsids are found in large aberrant perinuclear structures of the nuclear membranes suggests that NSF and the SNARE system are directly involved in virus-induced remodeling of nuclear membranes during nucleocapsid egress from the nucleus. Further studies to immunolocalize NSF and SNARE complexes within infected cells should shed light on whether the observed phenomena at the nuclear membrane result from direct or indirect effects. As the mechanism of nuclear egress is not known, it is possible that SNARE complexes play a direct role in the pinching off of vesicles containing progeny nucleocapsids during nuclear egress or in the release of nucleocapsids into the cytoplasm after nuclear egress.

Because a number of recent studies found that certain highly conserved or core AcMNPV genes (*ac11*, *ac76*, *ac78*, *ac80 or gp41*, *ac93*, *ac103*, *ac142*, and *ac146*) are required for infectious BV production and knockouts of these genes result in reduced nucleocapsid egress from the nucleus (41–45, 47, 48, 59), we examined their potential associations with NSF. We found that five of these conserved (core) proteins (Ac76, Ac78, GP41, Ac93, and Ac103) associated directly or indirectly (perhaps in larger complexes) with NSF. Predicted structure analysis indicated that, different from the predominant β-sheet composition of Ac11, Ac142, and Ac146, the other five examined viral proteins only contain 3 to 6 α-helixes (data not shown). The potential structure difference implies the interaction specificity of these viral proteins with NSF. As such, we speculate that these viral proteins associate in an egress complex on nuclear membranes. The associations of these viral proteins with NSF may contribute to the detection of NSF at what appear to be low levels in BV preparations (Fig. 12). While NSF was not detected in BV of AcMNPV in a prior proteomics analysis (32), NSF was identified in BV of another baculovirus, Helicoverpa armigera NPV (HaNPV) (50). Because of the low levels of NSF detected in BV, further studies will be required to determine whether NSF plays a functional role in BV.

Our studies reveal the importance of the cellular SNARE system in AcMNPV infection and the critical role of NSF in efficient BV entry and nuclear egress. A hypothetical model (Fig. 13) illustrates the potential bottlenecks to viral entry and egress and points of potential inhibition by DN NSF. Further studies will be necessary to define the precise roles of specific SNARE proteins in AcMNPV infection and to better characterize the interactions between components of the SNARE system and viral proteins. Overall,
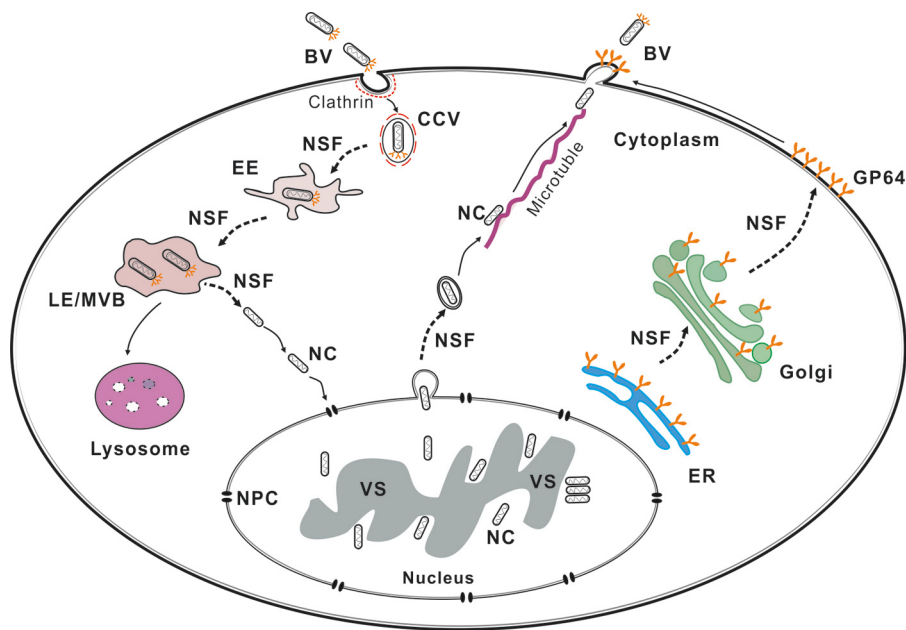
FIG 13 Hypothetical model for the role of cellular NSF protein in the infection cycle of AcMNPV. Steps at which NSF is potentially required for trafficking during budded virion entry and progeny nucleocapsid egress are indicated as dashed lines. BV, budded virions; CCV, clathrin-coated vesicles; EE, early endosome; ER, endoplasmic reticulum; LE, late endosome; MVB, multivesicular bodies; NC, nucleocapsid; NPC, nuclear pore complex; NSF, N-ethylmaleimide-sensitive factor; VS, virogenic stroma.

these studies should shed light on understanding the complex interplay between baculoviruses and the host cell trafficking pathways and proteins during viral entry and egress.

MATERIALS AND METHODS

Annotation of insect SNARE genes. SNARE genes of the yeast *Saccharomyces cerevisiae* and the orthologs from the human genome were used for searches of insect genomes using BLASTP and TBLASTN programs. BLAST searches were performed using databases of sequenced insect genomes from 6 orders, including Coleoptera (*Tribolium castaneum*; http://metazoa.ensembl.org/Tribolium _castaneum/Info/Index), Diptera (*Drosophila melanogaster*, *Aedes aegypti*, *Anopheles gambiae*, and *Culex quinquefasciatus*; http://flybase.org and http://www.vectorbase.org), Hemiptera (*Acyrthosiphon pisum*; http://www.aphidbase.com), Hymenoptera (*Apis mellifera*, *Nasonia vitripennis*, and *Harpegnathos saltator*; http://hymenopteragenome.org), Lepidoptera (*Bombyx mori* and *Danaus plexippus*; http://silkworm .genomics.org.cn and http://monarchbase.umassmed.edu), and Phthiraptera (*Pediculus humanus corporis*; http://www.vectorbase.org). Specific BLAST searches were also carried out at the National Center for Biotechnology Information (NCBI).

Cells, transfections, and infections. *Spodoptera frugiperda* Sf9, *Trichoplusia ni* Tn5B1-4 (High 5), and Sf9^{Op1D} (a cell line stably expressing Orgyia pseudotsugata MNPV [OpMNPV] GP64 [60]) cells were cultured at 27°C in TNMFH medium (Sigma-Aldrich) containing 10% fetal bovine serum (FBS; Gibco). The cells in 6-well plates (1×10^6 cells per well) or 12-well plates (2×10^5 cells per well) were transfected with plasmid or bacmid DNA or dsRNA using a $CaPO_4$ precipitation method (28). For virus infections, virus inoculum was added to cells and incubated for 1 h. The cells were washed once in TNMFH. Times postinfection were calculated from the time the viral inoculum was added.

NSF cDNA cloning. Total RNA was extracted from Sf9 cells by using an RNAiso plus kit (TaKaRa). The first-strand DNA complementary to the mRNA (cDNA) was synthesized by using avian myeloblastosis virus (AMV) reverse transcriptase and an oligo(dT) primer according to the manufacturer's instructions (TaKaRa). Gene-specific primers SfNsfF, SFNsfR, NsfF, and NsfR (Table 2), targeted to the Sf9 NSF ORF and the C terminus of Sf9 NSF ORF, were designed based on the EST sequences at the SPODOBASE database (http://bioweb.ensam.inra.fr/spodobase) (61). The PCR-amplified NSF ORF and a 90-bp fragment of NSF products were separately cloned into pMD18-T vector (TaKaRa) and sequenced with M13-47, M13-48, and NSF-specific primers. The pMD18-T vectors containing the ORF of NSF and the small fragment of NSF were designated NSFpMD18 and NSF90pMD18.

Analysis of the transcription of NSF. Sf9 cells in 6-well plates (1×10^6 cells per well) were infected with wild-type AcMNPV at an MOI of 10. At 1, 3, 6, 12, 18, 24, 36, and 48 h p.i., the infected and uninfected cells were collected and total RNA was extracted by using an RNAiso plus kit (TaKaRa). The genomic DNA elimination and cDNA synthesis were performed with a PrimeScript RT reagent kit with gDNA eraser and an oligo(dT) primer (TaKaRa). The transcript of NSF was quantified by real-time PCR (IQ5 multicolor

TABLE 2 PCR primers

Primer	Sequence (5′ to 3′)	Description
SfNsfF	ATGTCTGCAATGCGGATGAAG	Amplification of the ORF of Sf9 NSF
SfNsfR	TTATTGTACATTGGTGCCTAGGTC	
SfNsfXF	AATTCTAGAATGTCTGCAATGCGGATGAAG	Amplification of the ORF of Sf9 NSF
SfNsfER	AATGAATTCTGATTGTACATTGGTGCCTAGGTC	
NsfF	ACCGCCTTAGCCGCTGAACT	Amplification of 90 bp of Sf9 NSF
NsfR	AGACTCCGTGAATCCGACCATGT	
E329QF	CAGATCGACGCTATTTGCAAAGC	Construction of E329Q and R385A mutants
E329QR	GCAAATAGCGTCGATCTGGTCAAAGATGATAATGTGGA	
R385AF	GCTCCCGGTGCTCGAGGTTC	
R385AR	CTCGAGACGACCGGAGCCATCAACGCCTCGTCAATCAT	
HANmF	AATGAATTCTACCCATACGATGTTCCAGATTACGGTGGGACGTCGGGTGGAAGCGGTATGGTGAGCAAGGGCGAGGA	Construction of HA-NmpBlue
NmFt	CGAGCGGATGTACCCCGAGGACTAAATGTAATAATAAAAATTGTATCA	
NmRt	TGATACAATTTTTATTATTACATTTAGTCCTCGGGGTACATCCGCTCG	
64pAR	ATTAAGCTTCACACTCGCTATTTGGAACAT	
MycCmF	AATGAATTCGAACAAAAACTCATCTCAGAAGAGGATCTGGGGACGTCGGGTGGAAGCGGTGGCGCCCTGAAGGGCGAGATC	Construction of Myc-CmpBlue
CmFt	CGGCATGGACGAGCTGTACAAGTAGATGTAATAATAAAAATTGTATCA	
CmRt	TGATACAATTTTTATTATTACATCTACTTGTACAGCTCGTCCATGCCG	
64pAR	ATTAAGCTTCACACTCGCTATTTGGAACAT	
NmHAF	AATTCTAGAATGGTGAGCAAGGGCGAGGAG	Construction of Nm-HApBlue
NmHAR	ATTGGATCCAGCGTAATCTGGAACATCGTATGGGTAACCGCTTCCACCCGAGCGTCCCGTCCTCGGGGTACATCCGCTCG	
CmMycF	AATTCTAGAATGGGCGCCCTGAAGGGCGAGATC	Construction of Cm-MycpBlue
CmMycR	AATGGATCCCAGATCCTCTTCTGAGATGAGTTTTGTTCACCGCTTCCACCCGACGTCCCCTTGTACAGCTCGTCCATGCCG	
nMycF	CTAGAATGGAACAAAAACTCATCTCAGAAGAGGATCTGAATG	Construction of pIE-Myc-MCS
nMycR	GATCCATTCAGATCCTCTTCTGAGATGAGTTTTGTTCCATT	
nHaF	CTAGAATGTACCCATACGATGTTCCAGATTACGCTG	Construction of pIE-HA-MCS
nHaR	GATCCAGCGTAATCTGGAACATCGTATGGGTACATT	
cMycF	ATAAGAATTCGAACAAAAACTCATCTCAGAAGAGGATCTGAATTAGATGTAATAATAAAAATTGTATCA	Construction of pIE-MCS-Myc
64pAR	ATTAAGCTTCACACTCGCTATTTGGAACAT	
cHAF	ATAAGAATTCTACCCATACGATGTTCCAGATTACGCTTAGATGTAATAATAAAAATTGTATCA	Construction of pIE-MCS-HA
64pAR	ATTAAGCTTCACACTCGCTATTTGGAACAT	
NSFiF	GGATCCTAATACGACTCACTATAGGGACTCGCCAGCCCTAACAAAGA	Amplification of the dsDNA of Sf9 NSF
NSFiR	GGATCCTAATACGACTCACTATAGGGCGTTCAGTAGCCCTTGCTTG	
GFPiF	GGATCCTAATACGACTCACTATAGGACGTAAACGGCCACAAGTTC	Amplification of the dsDNA of GFP
GFPiR	GGATCCTAATACGACTCACTATAGGTGTTCTGCTGGTAGTGGTCG	

TABLE 3 Plasmids constructed in this study

Purpose	Construct name[a]
Expression and subcellular localization of NSF and its mutants	NSF-GFPpBlue
	E329Q-GFPpBlue
	R385A-GFPpBlue
Real-time PCR	NSF90pMD18
Coimmunoprecipitation	GP41-MycpBlue
	Lef3-MycpBlue
	NSF-MycpBlue
	Ac11-HApBlue
	Ac76-HApBlue
	Ac78-HApBlue
	GP41-HApBlue
	Ac93-HApBlue
	Ac103-HApBlue
	Ac142-HApBlue
	HA-Ac146pBlue
BiFC assay	NSF-HA-NmpBlue
	Ac11-HA-NmpBlue
	Ac76-HA-NmpBlue
	Ac78-HA-NmpBlue
	GP41-HA-NmpBlue
	Ac93-HA-NmpBlue
	Ac103-HA-NmpBlue
	Ac142-HA-NmpBlue
	Nm-HA-Ac146pBlue
	NSF-Myc-CmpBlue
	Ac11-Myc-CmpBlue
	Ac76-Myc-CmpBlue
	Ac78-Myc-CmpBlue
	GP41-Myc-CmpBlue
	Ac93-Myc-CmpBlue
	Ac103-Myc-CmpBlue
	Ac142-Myc-CmpBlue
	Lef3-Myc-CmpBlue
	Cm-Myc-Ac146pBlue

[a]Nm and Cm represent the N and C termini of mCherry, respectively.

real-time PCR detection system; Bio-Rad). Each PCR mixture contained 5 μl SYBR green premix *Ex Taq* II (TaKaRa), 1.25 μM each primer, and 500 pg of the cDNA template. Primers NsfF (5′-ACCGCCTTAGCCG CTGAACT-3′) and NsfR (5′-AGACTCCGTGAATCCGACCATGT-3′) were used to amplify a fragment of 90 bp of Sf9 NSF. Thermal cycling conditions were one cycle of 95°C for 3 min, followed by 40 cycles of 95°C for 10 s and 60°C for 45 s. A standard curve was generated by a serial dilution of NSF90pMD18. The transcript levels of NSF were expressed as numbers of transcript copies per cell.

Mutagenesis and construction of plasmids, bacmids, and viruses. PCR primers and the plasmid constructs are listed in Tables 2 and 3, respectively. The ORF of NSF containing a translation stop codon mutation (TAA to TAC) was generated by PCR using NSFpMD18 as the template and primers SfNsfXF and SfNsfER, which contain XbaI and EcoRI sites, respectively. The PCR product was digested with XbaI and EcoRI and inserted into the plasmid Vps4-GFPpBlue (62) under the control of the AcMNPV *ie1* immediate-early/late promoter to replace Vps4 and yield the C-terminal GFP-tagged NSF transient expression plasmid NSF-GFPpBlue. Two point mutations, E329Q and R385A, were separately introduced into NSF by overlap PCR using NSFpMD18 as a template and primers NsfE329QF, NsfE329QR, NsfR385AF, and NsfR385AR. The PCR products were digested with XbaI and EcoRI and cloned into the plasmid Vps4-GFPpBlue to replace Vps4 and yield NSF^{E329Q}-GFPpBlue and NSF^{R385A}-GFPpBlue. All of the plasmids were confirmed by restriction enzyme analysis and DNA sequencing. The previously constructed gfppBlue (62) was used as a GFP-expressing control plasmid.

To construct a bimolecular fluorescent complementation (BiFC) system, the ORF of mCherry was separated as two fragments between amino acid positions 159 and 160 as described previously (63). A backbone expression plasmid, pIE, was generated by inserting a multiple cloning site (MCS; 5′TCTAGAATG GGATCCACTAGTCCGCGGCCCGGGCTGCAGGATATCGAATTC3′) into the XbaI and EcoRI sites of pBiepA (64) to replace the ORF of GP64. The N- and C-terminal fragments of mCherry (designated Nm and Cm) containing the linker sequence GTSGGSG and the HA or c-Myc epitope tag were amplified by PCR using mCherryGUS bacmid DNA (62) as the template and inserted into the XbaI and BamHI or the XbaI and EcoRI sites of pIE to generate the BiFC expression plasmids Nm-HApBlue, HA-NmpBlue, Cm-MycpBue, and Myc-CmpBlue (Table 3). The immunoprecipitation vectors pIE-HA-MCS, pIE-Myc-MCS, pIE-MCS-HA,

and pIE-MCS-Myc, which contain the HA or c-Myc epitope tag, were constructed in a similar manner (Table 3). The NSF coding region, obtained by digesting NSF-GFPpBlue with XbaI and EcoRI, was inserted into the MCS of the BiFC and immunoprecipitation vectors. AcMNPV genes (ac11, ac76, ac78, ac80 [gp41], ac93, ac103, ac142, ac146, and lef3) were amplified by PCR and digested with XbaI and EcoRI or BamHI and EcoRI, and then the coding region of each viral gene was also inserted into the MCS of the vectors as described above (Table 3). All of the plasmids were confirmed by DNA sequencing.

Recombinant AcMNPV bacmids expressing GFP, GFP-tagged NSF (WT or with mutations), and c-Myc tagged NSF were constructed by inserting a cassette containing GFP, NSF-GFP, NSF^{E329Q}-GFP, NSF^{R385A}-GFP, or NSF-Myc under the control of the AcMNPV ie1 promoter into a pFastbac plasmid (GUSpFB) that contains a β-glucuronidase (GUS) gene under the control of the AcMNPV p6.9 late promoter. The resulting pFastbac constructs were each inserted into the polyhedrin locus of an AcMNPV bacmid (bMON14272) by Tn7-mediated transposition (65). The resulting recombinant bacmids were separately named GFPBac, NSF-GFPBac, NSF^{E329Q}-GFPBac, NSF^{R385A}-GFPBac, and NSF-MycBac. All constructs were verified by DNA sequencing. The gp64 knockout AcMNPV bacmids, LacZGUS-gp64^{ko} and mCherryGUS-gp64^{ko}, were constructed as described earlier (62). Plasmids and bacmids were purified using a Midiprep kit (Invitrogen). The gp64 knockout viruses, LacZGUS-gp64^{ko} and mCherryGUS-gp64^{ko}, were grown and their titers determined in Sf9^{OP1D} cells that constitutively express OpMNPV GP64 (60). Wild-type AcMNPV encoding VP39-triple mCherry (AcMNPV-3mC) (29) was kindly provided by Taro Ohkawa and Matthew Welch (University of California, Berkeley).

Cell viability assay. Cell viability, upon overexpression of NSF or the NSF DN constructs NSF^{E329Q} and NSF^{R385A}, was assessed using the CellTiter 96 AQueous one-solution cell proliferation assay (MTS; Promega) according to the manufacturer's recommendations. Briefly, Sf9 cells in 6-well plates were transfected with 3 μg of the plasmid expressing GFP, NSF-GFP, NSF^{E329Q}-GFP, or NSF^{R385A}-GFP. At 12, 24, and 36 h posttransfection (p.t.), the cells were incubated with CellTiter 96 AQueous one-solution reagent for 2 h at 27°C, and absorbance at 490 nm was monitored using a 96-well plate reader (iControl reader; Tecan, Mannedorf, Switzerland).

Infectivity complementation assay. Sf9 and High 5 cells in 6-well plates were cotransfected with 3 μg of pBieGP64 (64) expressing GP64 and 3 μg of a plasmid expressing GFP, NSF-GFP, NSF^{E329Q}-GFP, or NSF^{R385A}-GFP (typically, we observed that about 70 to 80% of cells showed GFP signals at 24 h posttransfection). At 12 h p.t., cells were infected with the GP64 knockout virus mCherryGUS-gp64^{ko} at a multiplicity of infection (MOI) of 1 or 5. At 24 h p.i., the supernatants and cells were separately collected and virus titers were measured by 50% tissue culture infectious dose (TCID$_{50}$) assays on Sf9^{OP1D} cells. Cell samples were analyzed for the expression of GP64, NSF, and its DN mutants by Western blotting.

RNAi assay. The dsRNA-based RNA interference (RNAi) assay was performed as described previously (66), with modifications. A 315-bp or 495-bp fragment of the coding sequence of Sf9 NSF or GFP was amplified by PCR. The PCR primers were designed with the SnapDragon tool (http://www.flyrnai.org/cgi-bin/RNAi_find_primers.pl), and each primer contained the T7 RNA polymerase promoter sequence (5'-TAATACGACTCACTATAGGG-3') at the 5' end (Table 2). The PCR products were purified using a QIAEXII gel extraction kit (Qiagen). The purified PCR products were used as templates to produce dsRNA by using the T7 RiboMAX express RNAi system (Promega). The dsRNA products were purified with an RNeasy minikit (Qiagen) and analyzed by 1.2% agarose gel electrophoresis.

Sf9 cells in 12-well plates were transfected with 7.5 μg of dsRNA targeting NSF or 7.5 μg of the GFP dsRNA as a negative control. At 24, 48, and 72 h p.t., cell viability was determined as described above. NSF knockdown efficiency was determined by transfecting Sf9 cells with 2 μg of the plasmid NSF-MycpBlue that expresses Myc-tagged NSF or cotransfecting Sf9 cells with 2 μg of NSF-MycpBlue and either (i) 7.5 μg of dsRNA targeting NSF or (ii) 7.5 μg dsRNA targeting GFP. At 24 and 48 h p.t., the transfected and cotransfected cells were collected and the expression of NSF-Myc was determined by Western blotting. Quantities of proteins on Western blots were estimated by using Quantity One software. For analysis of virus infection, Sf9 cells were transfected with 7.5 μg of dsRNA targeting NSF or 7.5 μg of the GFP dsRNA. At 48 h p.t., the cells were infected with wild-type (WT) AcMNPV at an MOI of 5. At 24 h p.i., the supernatants were collected and virus titers were measured by TCID$_{50}$ assays on Sf9 cells.

Analysis of viral gene expression and DNA replication. To determine the effects of dominant-negative NSF proteins on viral gene expression, Sf9 cells in 6-well plates were cotransfected with 3 μg of pBieGP64 expressing GP64 and 3 μg of a plasmid expressing NSF-GFP, NSF^{E329Q}-GFP, NSF^{R385A}-GFP, or the control GFP protein. At 12 h p.t., the cells were infected with the gp64 knockout virus LacZGUS-gp64^{ko} at an MOI of 5. At 6 and 24 h p.i., the infected cells were lysed with 0.5% NP-40 in phosphate-buffered saline (PBS) (pH 7.4), and the β-galactosidase or β-glucuronidase activities were measured using the substrate chlorophenol red-β-D-galactopyranoside (CPRG; Roche Diagnostics GmbH) or 4-nitrophenyl β-D-glucuronide (PNPG; Sigma-Aldrich) by absorbance at 570 nm (CPRG) or 405 nm (PNPG).

To evaluate the effects of DN NSF proteins on viral DNA replication, Sf9 cells were cotransfected with the plasmids described above (3 μg of each) and then infected at 12 h p.t. with gp64 knockout virus LacZGUS-gp64^{ko} (MOI of 5). At 24 h p.i., total DNA was extracted from infected cells using a DNeasy blood tissue kit (Qiagen). Viral genomic DNA was quantified by real-time PCR (IQ5 multicolor real-time PCR detection system; Bio-Rad). Each PCR mixture contained 5 μl SYBR premix Ex Taq II (TaKaRa), 1.25 μM each primer, and 500 pg of the DNA template. Primers ODV-e56F (5'-GATCTTCCTGCGGGCCAAACACT-3') and ODV-e56R (5'-AACAAGACCGCGCCTATCAACAAA-3') were used to amplify a fragment of 183 bp of the AcMNPV ODV-e56 gene as described previously (62). Thermal cycling conditions were one cycle of 95°C for 3 min, followed by 40 cycles of 95°C for 10 s and 60°C for 45 s. A standard curve was generated

by a serial dilution of ODV-e56pGEM, which contains the ODV-e56 ORF (62). AcMNPV genomic DNA was expressed as numbers of viral DNA copies per cell.

Analysis of virus entry. Sf9 cells in 6-well plates were transfected with 3 μg of the plasmid GFP-pBlue, NSF-GFPpBlue, NSF^{E329Q}-GFPpBlue, or NSF^{R385A}-GFPpBlue. At 12 h p.t., the cells were prechilled at 4°C for 30 min and then incubated with mCherry-labeled virions of AcMNPV-3mC (MOI of 10 or 20 TCID$_{50}$) at 4°C for 1 h. After removing the virus inoculum, cells were washed twice with cold TNMFH medium and shifted to 27°C for 60 min. One set of cells (which were infected at an MOI of 10) were used for extraction of total DNA, and viral genomic DNA was quantified by real-time PCR as described above. The other set of cells (which were infected at an MOI of 20) was fixed with 3.7% paraformaldehyde in PBS (pH 7.4) and analyzed by confocal microscopy as described below.

Analysis of virus egress. To examine the effects of DN NSF on infectious budded virion production, Sf9 cells in 6-well plates were transfected with 3 μg of recombinant AcMNPV bacmid GFP-Bac, NSF-GFPBac, NSF^{E329Q}-GFPBac, or NSF^{R385A}-GFPBac, which express NSF or control genes under an ie1 promoter. At 24 h p.t., GFP-positive cells were counted under an epifluorescence micro-scope (Nikon Eclipse Ti) to evaluate the transfection efficiency. Transfected cells were also solubilized with 0.5% NP-40 in PBS (pH 7.4), and GUS activities were measured as described above. The cell supernatants were collected and infectious virus titers were determined by TCID$_{50}$ assays on Sf9 cells.

Confocal microscopy and imaging. Transfected and/or infected Sf9 cells were prepared on glass coverslips and fixed with 3.7% paraformaldehyde in PBS (pH 7.4) for 10 min and permeabilized with 0.05% Triton X-100 in PBS (pH 7.4) for 1 min. The nuclei were then stained with 1 μg/ml Hoechst 33258 (Invitrogen) for 8 min. After washing four times with PBS (pH 7.4), the cells were mounted on slides in Fluoromount-G reagent (Southern Biotech). Images were collected on a Nikon A1R confocal microscope (Nikon Instruments Inc., Melville, NY, USA) with a 60× oil immersion objective (numeric aperture, 1.4). GFP was excited with a blue argon ion laser (488 nm), and emitted light was collected between 480 and 520 nm. mCherry was excited with an orange helium-neon laser (594 nm), and emitted light was collected from 580 to 650 nm. Hoechst 33258 was excited with UV light at approximately 350 nm, and emitted light was collected from 400 nm to 450 nm. GFP and mCherry signals were collected separately from the Hoechst 33258 signal and later superimposed. Images were processed using Nikon NIS-Elements AR software (version 4.0) and Adobe Photoshop CC (version 14.0) (Adobe Systems).

cELISA, immunofluorescence, and syncytium formation assay. Sf9 cells in 12-well plates were transfected with 2.5 μg of the bacmid (GFP-Bac, NSF^{E329Q}-GFPBac, or NSF^{R385A}-GFPBac) or 0.5 to 2.5 μg NSF-GFPBac. At 24 h p.t., the supernatant was collected and the infectious BV titers were determined by TCID$_{50}$ assay. Two sets of transfected cells were separately fixed with either 0.5% glutaraldehyde or 3.7% paraformaldehyde and analyzed by cELISA or immunofluorescence using anti-GP64 monoclonal anti-body AcV5 or AcV1, respectively. Another set of cells was treated with PBS (pH 5.0) for 3 min to induce syncytium formation. The cells in syncytia (containing ≥5 nuclei) were scored. ELISA, immunofluores-cence, and syncytium formation assays were carried out as described previously (64).

Transmission electron microscopy. Sf9 cells in 6-well plates were transfected with 6 μg of each bacmid (NSF-GFPBac, NSF^{E329Q}-GFPBac, or NSF^{R385A}-GFPBac). At 48 h p.t., the cells were harvested by centrifugation (500 × g, 10 min) and fixed with 2.5% glutaraldehyde in PBS (pH 7.4) overnight at 4°C. Cells were then washed five times with PBS buffer (0.1 M, pH 7.2) and stained with 1% osmium tetroxide in PBS buffer (0.2 M, pH 7.2) for 2 h at 4°C. After rinsing five times in PBS buffer (0.1 M, pH 7.2), the samples were dehydrated stepwise with a gradient of ethanol from 30% to 100%. The samples were then embedded in Epon-812 and dried for about 48 h at 55°C. Ultrathin sections were prepared and stained with lead citrate and uranyl acetate. Images were collected with an HT7700 transmission electron microscope (Hitachi, Ltd., Japan).

Coimmunoprecipitation. Sf9 cells in 12-well plates were transfected or cotransfected with the plasmids expressing HA-tagged GP41 and/or c-Myc-tagged GP41 or Lef3 or plasmids expressing c-Myc-tagged NSF and/or HA-tagged viral proteins (2 μg of each plasmid). At 36 h p.t., the cells were lysed in radioimmunoprecipitation assay (RIPA) buffer (0.1% SDS, 50 mM Tris, pH 8.0, 150 mM NaCl, 5 mM EDTA, 0.5% sodium deoxycholate, 1% NP-40) containing protein inhibitor cocktail (Roche) at 4°C for 10 min. The supernatant then was collected and debris removed by centrifugation (15,000 × g, 15 min, 4°C). For immunoprecipitation, the lysate supernatants were mixed with anti-HA monoclonal antibodies for 4 h at 4°C, and then the mixture was incubated with protein G agarose beads (Pierce) overnight at 4°C. After pelleting and washing twice with RIPA buffer, the agarose beads were resuspended with 1× SDS-PAGE gel loading buffer (2% SDS, 10% glycerol, 2% β-mercaptoethanol, 0.02% bromophenol blue, 0.05 M Tris, pH 6.8), heated at 100°C for 5 min, and analyzed by 10% or 15% SDS-PAGE and Western blotting.

BiFC assay. Sf9 cells in 12-well plates were cotransfected with the BiFC plasmid pairs (2 μg of each plasmid) expressing the specific protein fused with the N or C terminus of mCherry (Nm or Cm, respectively). At 36 h p.t., bimolecular fluorescent complementation was examined by observing mCherry fluorescence in transfected cells with a Nikon Eclipse Ti epifluorescence microscope. In five randomly selected representative fields, the numbers and percentages of mCherry-positive cells were calculated for each pair of constructs. The protein pair associations were estimated by the ratio of the number of fluorescent cells in the field compared to the total number of cells in that field as described previously (67). Expression of the target proteins was confirmed in transfected cells by Western blotting.

BV purification. The purification of budded virions (BV) was performed as described previously (62). Briefly, Sf9 cells in 6-well plates were transfected with 6 μg of NSF-MycBac DNA. At 72 h p.t., the infected cell supernatants were collected and cell debris removed by centrifugation at 4°C for 10 min at 3,000 × g. The supernatant was loaded onto a 25% (wt/vol) sucrose cushion and centrifuged (4°C, 90 min, 28,000 rpm; Himac P28S rotor). Virus pellets were resuspended in PBS (pH 6.2), overlaid onto a 30 to 55%

(wt/vol) continuous sucrose gradient, and centrifuged (4°C, 90 min, 28,000 rpm; Himac P40ST rotor). The virus fraction was collected and diluted (1:10) with PBS (pH 6.2) and centrifuged at 28,000 rpm for 90 min at 4° (Himac P40ST rotor). BV pellets were resuspended in PBS (pH 6.2) with protease inhibitor cocktail (Roche) and subjected to Western blot analysis.

Western blot analysis. Virion and cell lysates were separated on 6%, 10%, or 15% reducing or nonreducing polyacrylamide gels and transferred to polyvinylidene difluoride (PVDF) membrane (Millipore) as described previously (36). GFP, GFP-tagged proteins, c-Myc-tagged proteins, and AcMNPV VP39 were separately detected with anti-GFP (GenScript), anti-Myc (EarthOx, L.L.C.), or anti-VP39 polyclonal antibody (68). HA-tagged proteins, GUS, or actin were detected with anti-HA (EarthOx, L.L.C.), anti-GUS (BGI), or anti-β-actin monoclonal antibodies (Abbkine). Immunoreactive proteins were visualized using alkaline phosphatase-conjugated anti-mouse or anti-rabbit IgG antibody and nitroblue tetrazolium–5-bromo-4-chloro-3-indolylphosphate (NBT-BCIP; Promega).

Accession number(s). The *Spodoptera frugiperda* NSF gene was deposited in GenBank under accession number KY548397.

SUPPLEMENTAL MATERIAL

Supplemental material for this article may be found at https://doi.org/10.1128/JVI.01111-17.

SUPPLEMENTAL FILE 1, PDF file, 0.2 MB.

ACKNOWLEDGMENTS

REFERENCES

1. Jahn R, Scheller RH. 2006. SNAREs– engines for membrane fusion. Nat Rev Mol Cell Biol 7:631–643. https://doi.org/10.1038/nrm2002.
2. Weber T, Zemelman BV, McNew JA, Westermann B, Gmachl M, Parlati F, Sollner TH, Rothman JE. 1998. SNAREpins: minimal machinery for membrane fusion. Cell 92:759–772. https://doi.org/10.1016/S0092-8674(00)81404-X.
3. Fasshauer D, Sutton RB, Brunger AT, Jahn R. 1998. Conserved structural features of the synaptic fusion complex: SNARE proteins reclassified as Q- and R-SNAREs. Proc Natl Acad Sci U S A 95:15781–15786. https://doi.org/10.1073/pnas.95.26.15781.
4. Kloepper TH, Kienle CN, Fasshauer D. 2007. An elaborate classification of SNARE proteins sheds light on the conservation of the eukaryotic endomembrane system. Mol Biol Cell 18:3463–3471. https://doi.org/10.1091/mbc.E07-03-0193.
5. Sollner T, Bennett MK, Whiteheart SW, Scheller RH, Rothman JE. 1993. A protein assembly-disassembly pathway in-vitro that may correspond to sequential steps of synaptic vesicle docking, activation, and fusion. Cell 75:409–418. https://doi.org/10.1016/0092-8674(93)90376-2.
6. Mayer A, Wickner W, Haas A. 1996. Sec18p (NSF)-driven release of sec17p (alpha-SNAP) can precede docking and fusion of yeast vacuoles. Cell 85:83–94. https://doi.org/10.1016/S0092-8674(00)81084-3.
7. Zhao CX, Smith EC, Whiteheart SW. 2012. Requirements for the catalytic cycle of the N-ethylmaleimide-sensitive factor (NSF). Biochim Biophys Acta 1823:159–171. https://doi.org/10.1016/j.bbamcr.2011.06.003.
8. Block MR, Glick BS, Wilcox CA, Wieland FT, Rothman JE. 1988. Purification of an N-ethylmaleimide-sensitive protein catalyzing vesicular transport. Proc Natl Acad Sci U S A 85:7852–7856. https://doi.org/10.1073/pnas.85.21.7852.
9. Zhao M, Brunger AT. 2016. Recent advances in deciphering the structure and molecular mechanism of the AAA+ ATPase N-ethylmaleimide-sensitive factor (NSF). J Mol Biol 428:1912–1926. https://doi.org/10.1016/j.jmb.2015.10.026.
10. Whiteheart SW, Rossnagel K, Buhrow SA, Brunner M, Jaenicke R, Rothman JE. 1994. N-ethylmaleimide-sensitive fusion protein–a trimeric ATPase whose hydrolysis of ATP is required for membrane-fusion. J Cell Biol 126:945–954. https://doi.org/10.1083/jcb.126.4.945.
11. Tagaya M, Wilson DW, Brunner M, Arango N, Rothman JE. 1993. Domain-structure of an N-ethylmaleimide-sensitive fusion protein involved in vesicular transport. J Biol Chem 268:2662–2666.
12. Matveeva EA, May AP, He P, Whiteheart SW. 2002. Uncoupling the

ATPase activity of the N-ethylmaleimide sensitive factor (NSF) from 20S complex disassembly. Biochemistry 41:530–536. https://doi.org/10.1021/bi015632s.
13. Nagiec EE, Bernstein A, Whiteheart SW. 1995. Each domain of the N-ethylmaleimide-sensitive fusion protein contributes to its transport activity. J Biol Chem 270:29182–29188. https://doi.org/10.1074/jbc.270.49.29182.
14. Liu ST, Sharon-Friling R, Ivanova P, Milne SB, Myers DS, Rabinowitz JD, Brown HA, Shenk T. 2011. Synaptic vesicle-like lipidome of human cytomegalovirus virions reveals a role for SNARE machinery in virion egress. Proc Natl Acad Sci U S A 108:12869–12874. https://doi.org/10.1073/pnas.1109796108.
15. Kawabata A, Serada S, Naka T, Mori Y. 2014. Human herpesvirus 6 gM/gN complex interacts with v-SNARE in infected cells. J Gen Virol 95:2769–2777. https://doi.org/10.1099/vir.0.069336-0.
16. Ding BB, Zhang GY, Yang XD, Zhang SW, Chen LY, Yan Q, Xu MY, Banerjee AK, Chen MZ. 2014. Phosphoprotein of human parainfluenza virus type 3 blocks autophagosome-lysosome fusion to increase virus production. Cell Host Microbe 15:564–577. https://doi.org/10.1016/j.chom.2014.04.004.
17. Ren H, Elgner F, Jiang B, Himmelsbach K, Medvedev R, Ploen D, Hildt E. 2016. The autophagosomal snare protein syntaxin 17 is an essential factor for the hepatitis C virus life cycle. J Virol 90:5989–6000. https://doi.org/10.1128/JVI.00551-16.
18. Joshi A, Garg H, Ablan SD, Freed EO. 2011. Evidence of a role for soluble N-ethylmaleimide-sensitive factor attachment protein receptor (SNARE) machinery in HIV-1 assembly and release. J Biol Chem 286:29861–29871. https://doi.org/10.1074/jbc.M111.241521.
19. Garg H, Joshi A. 2012. SNAREs in HIV-1 assembly. Commun Integr Biol 5:172–174. https://doi.org/10.4161/cib.18742.
20. Pirooz SD, He SS, Zhang T, Zhang XW, Zhao Z, Oh S, O'Connell D, Khalilzadeh P, Amini-Bavil-Olyaee S, Farzan M, Liang CY. 2014. UVRAG is required for virus entry through combinatorial interaction with the class C-Vps complex and SNAREs. Proc Natl Acad Sci U S A 111:2716–2721. https://doi.org/10.1073/pnas.1320629111.
21. Meier R, Franceschini A, Horvath P, Tetard M, Mancini R, von Mering C, Helenius A, Lozach PY. 2014. Genome-wide small interfering RNA screens reveal VAMP3 as a novel host factor required for Uukuniemi virus late penetration. J Virol 88:8565–8578. https://doi.org/10.1128/JVI.00388-14.

22. Rohrmann GF. 2013. Baculovirus molecular biology, 3rd ed. National Center for Biotechnology Information, Bethesda, MD.

23. Haase S, Sciocco-Cap A, Romanowski V. 2015. Baculovirus insecticides in Latin America: historical overview, current status and future perspectives. Viruses 7:2230–2267. https://doi.org/10.3390/v7052230.

24. Sun X. 2015. History and current status of development and use of viral insecticides in China. Viruses 7:306–319. https://doi.org/10.3390/v7010306.

25. van Oers MM, Pijlman GP, Vlak JM. 2015. Thirty years of baculovirus-insect cell protein expression: from dark horse to mainstream technology. J Gen Virol 96:6–23. https://doi.org/10.1099/vir.0.067108-0.

26. Long G, Pan XY, Kormelink R, Vlak JM. 2006. Functional entry of baculovirus into insect and mammalian cells is dependent on clathrin-mediated endocytosis. J Virol 80:8830–8833. https://doi.org/10.1128/JVI.00880-06.

27. Li Z, Blissard GW. 2011. Autographa californica multiple nucleopolyhedrovirus GP64 protein: roles of histidine residues in triggering membrane fusion and fusion pore expansion. J Virol 85:12492–12504. https://doi.org/10.1128/JVI.05153-11.

28. Blissard GW, Wenz JR. 1992. Baculovirus GP64 envelope glycoprotein is sufficient to mediate pH-dependent membrane fusion. J Virol 66:6829–6835.

29. Ohkawa T, Volkman LE, Welch MD. 2010. Actin-based motility drives baculovirus transit to the nucleus and cell surface. J Cell Biol 190:187–195. https://doi.org/10.1083/jcb.201001162.

30. Au S, Pante N. 2012. Nuclear transport of baculovirus: revealing the nuclear pore complex passage. J Struct Biol 177:90–98. https://doi.org/10.1016/j.jsb.2011.11.006.

31. Fraser MJ. 1986. Ultrastructural observations of virion maturation in Autographa californica nuclear polyhedrosis virus infected Spodoptera frugiperda cell cultures. J Ultrastruct Mol Struct Res 95:189–195. https://doi.org/10.1016/0889-1605(86)90040-6.

32. Wang RR, Deng F, Hou DH, Zhao Y, Guo L, Wang HL, Hu ZH. 2010. Proteomics of the Autographa californica nucleopolyhedrovirus budded virions. J Virol 84:7233–7242. https://doi.org/10.1128/JVI.00040-10.

33. Chen YR, Zhong SL, Fei ZJ, Gao S, Zhang SY, Li ZF, Wang P, Blissard GW. 2014. Transcriptome responses of the host *Trichoplusia ni* to infection by the baculovirus Autographa californica multiple nucleopolyhedrovirus. J Virol 88:13781–13797. https://doi.org/10.1128/JVI.02243-14.

34. Zhao C, Matveeva EA, Ren Q, Whiteheart SW. 2010. Dissecting the N-ethylmaleimide-sensitive factor: required elements of the N and D1 domains. J Biol Chem 285:761–772. https://doi.org/10.1074/jbc.M109.056739.

35. Antonin W, Holroyd C, Fasshauer D, Pabst S, von Mollard GF, Jahn R. 2000. A SNARE complex mediating fusion of late endosomes defines conserved properties of SNARE structure and function. EMBO J 19:6453–6464. https://doi.org/10.1093/emboj/19.23.6453.

36. Oomens AGP, Blissard GW. 1999. Requirement for GP64 to drive efficient budding of Autographa californica multicapsid nucleopolyhedrovirus. Virology 254:297–314. https://doi.org/10.1006/viro.1998.9523.

37. Kadlec J, Loureiro S, Abrescia NG, Stuart DI, Jones IM. 2008. The post-fusion structure of baculovirus gp64 supports a unified view of viral fusion machines. Nat Struct Mol Biol 15:1024–1030. https://doi.org/10.1038/nsmb.1484.

38. Li Z, Blissard GW. 2010. Baculovirus GP64 disulfide bonds: the intermolecular disulfide bond of Autographa californica multicapsid nucleopolyhedrovirus GP64 is not essential for membrane fusion and virion budding. J Virol 84:8584–8595.

39. Oomens AG, Monsma SA, Blissard GW. 1995. The baculovirus GP64 envelope fusion protein: synthesis, oligomerization, and processing. Virology 209:592–603. https://doi.org/10.1006/viro.1995.1291.

40. Zhou J, Blissard GW. 2008. Identification of a GP64 subdomain involved in receptor binding by budded virions of the baculovirus Autographica californica multicapsid nucleopolyhedrovirus. J Virol 82:4449–4460. https://doi.org/10.1128/JVI.02490-07.

41. Tao XY, Choi JY, Kim WJ, Lee JH, Liu Q, Kim SE, An SB, Kim SE, Woo SD, Jin BR, Je YH. 2013. The Autographa californica multiple nucleopolyhedrovirus ORF78 is essential for budded virus production and general occlusion body formation. J Virol 87:8441–8450. https://doi.org/10.1128/JVI.01290-13.

42. Tao XY, Choi JY, Kim WJ, An SB, Liu Q, Kim SE, Lee SH, Kim JH, Woo SD, Jin BR, Je YH. 2015. Autographa californica multiple nucleopolyhedrovirus ORF11 is essential for budded-virus production and occlusion-derived-virus envelopment. J Virol 89:373–383. https://doi.org/10.1128/JVI.01742-14.

43. Olszewski J, Miller LK. 1997. A role for baculovirus GP41 in budded virus production. Virology 233:292–301. https://doi.org/10.1006/viro.1997.8612.

44. Dickison VL, Willis LG, Sokal NR, Theilmann DA. 2012. Deletion of AcMNPV ac146 eliminates the production of budded virus. Virology 431:29–39. https://doi.org/10.1016/j.virol.2012.05.002.

45. Hu ZY, Yuan MJ, Wu WB, Liu C, Yang K, Pang Y. 2010. Autographa californica multiple nucleopolyhedrovirus ac76 is involved in intranuclear microvesicle formation. J Virol 84:7437–7447. https://doi.org/10.1128/JVI.02103-09.

46. McCarthy CB, Dai XJ, Donly C, Theilmann DA. 2008. Autographa californica multiple nucleopolyhedrovirus ac142, a core gene that is essential for BV production and ODV envelopment. Virology 372:325–339. https://doi.org/10.1016/j.virol.2007.10.019.

47. Yuan MJ, Huang ZQ, Wei DH, Hu ZY, Yang K, Pang Y. 2011. Identification of Autographa californica nucleopolyhedrovirus ac93 as a core gene and its requirement for intranuclear microvesicle formation and nuclear egress of nucleocapsids. J Virol 85:11664–11674. https://doi.org/10.1128/JVI.05275-11.

48. Yuan MJ, Wu WB, Liu C, Wang YJ, Hu ZY, Yang K, Pang Y. 2008. A highly conserved baculovirus gene p48 (ac103) is essential for BV production and ODV envelopment. Virology 379:87–96. https://doi.org/10.1016/j.virol.2008.06.015.

49. Peng K, Wu M, Deng F, Song J, Dong C, Wang H, Hu Z. 2010. Identification of protein-protein interactions of the occlusion-derived virus-associated proteins of Helicoverpa armigera nucleopolyhedrovirus. J Gen Virol 91:659–670. https://doi.org/10.1099/vir.0.017103-0.

50. Hou DH, Zhang LK, Deng F, Fang W, Wang RR, Liu XJ, Guo L, Rayner S, Chen XW, Wang HL, Hu ZH. 2013. Comparative proteomics reveal fundamental structural and functional differences between the two progeny phenotypes of a baculovirus. J Virol 87:829–839. https://doi.org/10.1128/JVI.02329-12.

51. Xue J, Qiao N, Zhang W, Cheng RL, Zhang XQ, Bao YY, Xu YP, Gu LZ, Han JD, Zhang CX. 2012. Dynamic interactions between Bombyx mori nucleopolyhedrovirus and its host cells revealed by transcriptome analysis. J Virol 86:7345–7359. https://doi.org/10.1128/JVI.07217-12.

52. Salem TZ, Zhang F, Xie Y, Thiem SM. 2011. Comprehensive analysis of host gene expression in Autographa californica nucleopolyhedrovirus-infected *Spodoptera frugiperda* cells. Virology 412:167–178. https://doi.org/10.1016/j.virol.2011.01.006.

53. Granados RR, Lawler KA. 1981. In vivo pathway of Autographa californica baculovirus invasion and infection. Virology 108:297–308. https://doi.org/10.1016/0042-6822(81)90438-4.

54. Volkman LE, Goldsmith PA. 1985. Mechanism of neutralization of budded Autographa californica nuclear polyhedrosis virus by a monoclonal antibody: inhibition of entry by adsorptive endocytosis. Virology 143:185–195. https://doi.org/10.1016/0042-6822(85)90107-2.

55. Hefferon KL, Oomens AG, Monsma SA, Finnerty CM, Blissard GW. 1999. Host cell receptor binding by baculovirus GP64 and kinetics of virion entry. Virology 258:455–468. https://doi.org/10.1006/viro.1999.9758.

56. Fang MG, Nie YC, Theilmann DA. 2009. AcMNPV EXON0 (AC141) which is required for the efficient egress of budded virus nucleocapsids interacts with beta-tubulin. Virology 385:496–504. https://doi.org/10.1016/j.virol.2008.12.023.

57. Biswas S, Blissard GW, Theilmann DA. 2016. Trichoplusia ni kinesin-1 associates with Autographa californica multiple nucleopolyhedrovirus nucleocapsid proteins and is required for production of budded virus. J Virol 90:3480–3495. https://doi.org/10.1128/JVI.02912-15.

58. Baur T, Ramadan K, Schlundt A, Kartenbeck J, Meyer HH. 2007. NSF- and SNARE-mediated membrane fusion is required for nuclear envelope formation and completion of nuclear pore complex assembly in *Xenopus laevis* egg extracts. J Cell Sci 120:2895–2903. https://doi.org/10.1242/jcs.010181.

59. Li SN, Wang JY, Yuan MJ, Yang K. 2014. Disruption of the baculovirus core gene ac78 results in decreased production of multiple nucleocapsid-enveloped occlusion-derived virions and the failure of primary infection in vivo. Virus Res 191:70–82. https://doi.org/10.1016/j.virusres.2014.07.019.

60. Plonsky I, Cho MS, Oomens AGP, Blissard G, Zimmerberg J. 1999. An analysis of the role of the target membrane on the GP64-induced fusion pore. Virology 253:65–76. https://doi.org/10.1006/viro.1998.9493.

61. Negre V, Hotelier T, Volkoff AN, Gimenez S, Cousserans F, Mita K, Sabau X, Rocher J, Lopez-Ferber M, d'Alencon E, Audant P, Sabourault C, Bidegainberry V, Hilliou F, Fournier P. 2006. SPODOBASE: an EST

database for the lepidopteran crop pest Spodoptera. BMC Bioinformatics 7:322. https://doi.org/10.1186/1471-2105-7-322.

62. Li Z, Blissard GW. 2012. Cellular VPS4 is required for efficient entry and egress of budded virions of Autographa californica multiple nucleopolyhedrovirus. J Virol 86:459–472. https://doi.org/10.1128/JVI.06049-11.

63. Fan JY, Cui ZQ, Wei HP, Zhang ZP, Zhou YF, Wang YP, Zhang XE. 2008. Split mCherry as a new red bimolecular fluorescence complementation system for visualizing protein-protein interactions in living cells. Biochem Biophys Res Commun 367:47–53. https://doi.org/10.1016/j.bbrc.2007.12.101.

64. Li Z, Blissard GW. 2008. Functional analysis of the transmembrane (TM) domain of the Autographa californica multicapsid nucleopolyhedrovirus GP64 protein: substitution of heterologous TM domains. J Virol 82:3329–3341. https://doi.org/10.1128/JVI.02104-07.

65. Luckow VA, Lee SC, Barry GF, Olins PO. 1993. Efficient generation of infectious recombinant baculoviruses by site-specific transposon-mediated insertion of foreign genes into a baculovirus genome propagated in Escherichia coli. J Virol 67:4566–4579.

66. Deng Z, Huang Z, Yuan M, Yang K, Pang Y. 2014. Baculovirus induces host cell aggregation via a Rho/Rok-dependent mechanism. J Gen Virol 95:2310–2320. https://doi.org/10.1099/vir.0.066811-0.

67. Webster BM, Colombi P, Jager J, Lusk CP. 2014. Surveillance of nuclear pore complex assembly by ESCRT-III/Vps4. Cell 159:388–401. https://doi.org/10.1016/j.cell.2014.09.012.

68. Li L, Li Z, Chen W, Pang Y. 2007. Cloning, expression of Autographa californica nucleopolyhedrovirus vp39 gene in Escherichia coli and preparation of its antibody. Biotechnology 17:5–7.